Astronomy & Astrophysics manuscript no. liners-masegosa
November 4, 2010

The nature of nuclear H_α emission in LINERs

J. Masegosa[1], I. Márquez[1], A. Ramirez[1,2], and O. González-Martín[3,4]

[1] Instituto de Astrofísica de Andalucía (CSIC), Apdo. 3004, 18080 Granada, Spain ⋆
[2] Instituto de Astronomía de la Universidad Nacional Autónoma de México, Apdo. Postal 70-264 México D.F., México
[3] IESL, Foundation for Research and Technology, 711 10, Heraklion, Crete, Greece
[4] Physics Department, University of Crete, P.O. Box 2208, Gr-710 03 Heraklion, Crete, Greece

ABSTRACT

To get insight in the nature of the ionized gas in the nuclear region of LINERs we have performed a study of HST Hα imaging of 32 LINERs. The main conclusion from this analysis is that for the large majority of LINERs (84%) an unresolved nuclear source has been identified as well as extended emission with equivalent sizes ranging from few tens till about hundredths of parsecs. Their morphologies appear not to be homogeneous being basically grouped into three classes: nuclear outflow candidates (42%), core-halo morphologies (25%) and nuclear spiral disks (14%). Clumpy structures reminiscent of young stellar clusters are not a common property on LINERs. The remaining 5 galaxies are too dusty to allow a clear view of the ionized gas distribution.
A size-luminosity relation has been found between the equivalent radius of the Hα emission and the (2-10 keV) X-ray luminosities. Both ionised gas morphologies and the size-luminosity relation are indistinguishable from those of low luminosity Seyferts, suggesting the same origin for the NLR of LINERs and Seyferts. Also a relation between soft X-rays and ionized gas has been suggested for the first time in LINERs. From multiwavelength data, only 4 out of the 32 LINERs have no evidences on an AGN nature of their nuclear sources from multiwavelength data, but extremely obscured AGNs cannot be discarded out given the Compton thick signatures of their X-ray emission. For the confirmed AGN LINERs, their Hα imaging favour core-halo and outflow morphologies (65% of the cases). Finally, their calculated Eddington ratios show that our LINER sources radiate at sub-Eddington regime, with core-halo systems having on average larger Eddington ratios than outflow candidates.

Key words. Galaxies:active, Galaxies:nuclei, Galaxies:evolution,X-ray:galaxies

1. Introduction

It has been suggested that *Low Ionization nuclear emission-line regions* (LINERs, Heckman 1980) are placed at the low luminosity end among the active galactic nuclei (AGN) family (Ho 2008). Although LINERs are found in a large population of nearby galaxies (30%; Ho et al 1997), a debate still does exist on the nature of their energy source.

Ho (2002, 2008) summarizes the main lines of evidence supporting the AGN nature of LINERs: host galaxies properties similar to Seyferts, most of the more massive black holes residing in LINERs, incidence of broad line regions (hereinafter BLR), compact nuclei at both radio and X-ray frequencies. He atributes the large progress made during the last two decades to multifrequency analyses and HST high spatial resolution studies.

The extensive work made by Nagar et al. (2000, 2002, 2005) have shown that radio cores are found in 44% of LINERs, a percentage similar to that observed in Seyferts (47%). Also when radio data at different frequencies exist their spectra tend to be flat as it is expected when non-thermal processes take place.

At X-ray frequencies large progress has also been made thanks to the large X-ray facilities Chandra and XMM-Newton. X-ray observations can be considered of paramount importance, constituting one of the best tools to identify AGN. From the different studies carried out in the last decade (Ho et al. 2001, Eracleous et al. 2002, Dudik et al. 2005, González-Martín et al. 2006 and 2009a), it has been proved that an AGN is present in at least 60% of the LINERs. Moreover when multifrequency information is taken into account (basically the incidence of broad lines and the properties at radio frequencies) the percentage of AGNs rises up to 90% (González-Martín et al. 2006 and 2009a).

On their hand, HST observations have provided a large advance in the physics of LINERS. The pioneering UV imaging surveys by Maoz et al. (1995) and Barth et al. (1998) concluded that 25% of the observed LINERs had an UV compact source in their nuclei. But of course one of the most outstanding results during the last decade has been the discovery that sources with detected radiocores show variability at UV frequencies on month scales (Maoz 2007). Four of their 13 sources (namely M81, NGC 3998, NGC 4203 and NGC 4579) have been confirmed to be variable also at X-ray frequencies (Pian et al. 2010). Recently González-Martín et al. (2010) have also detected X-ray variability for the LINER NGC 4102.

HST optical works (Pogge et al. 2000; Simões Lopes et al. 2007; González-Delgado et al. 2008; González-Martín et al. 2009a) have confirmed that almost all the observed LINERs show a nuclear source on top of an irregular distribution of circumnuclear dust. Dust obscuration can explain the existence of dark-UV LINERs. The importance of an obscuring environment, maybe linked to the acretion physiscs, has been recognized in our X-ray aproach to the nature of LINERs (González- Martín et al. 2009b). We found that a large percentage of them (50%) show clear signs to be Compton thick. This fraction is even larger than that reported for Seyferts (30%) (González-Martín et al. 2009b, Panessa et al. 2006) and so the location and nature of their obscuring matter needs to be further investigated. Until new high resolution X-ray images become available, only indirect information can be obtained on the nature of LINERs by looking for

⋆ e-mail: pepa@iaa.es

correlations between X-ray properties taken at lower resolution and optical/NIR properties taken at much larger spatial resolution. In this vein, it is worthwhile to search for the properties of the ionized gas and its relation to the X-ray results.

Previous works have concluded that the Hα morphology of LINERs mainly consists on a point source embeded in an extended structure sometimes clumpy, filamentary and in some particular cases with clear indications of nuclear obscuration, but mostly indistinguishable from what is observed in low luminosity Seyfert galaxies (Pogge et al. 2000, Chiaberge et al. 2005 and Dai & Wang 2008). Based on STIS spectroscopic observations of 13 LINERs, Walsh et al. (2008) clearly demonstrate that at scales of tens of parsecs their energy source is consistent with photoionization by the central nuclear source, but with a NLR kinematics dominated by outflows. Following Barth's (2002) considerations, by analogy with Seyfert unification models, it is natural to wonder whether the various types of low luminosity AGN (LLAGN), which LINERs could belong to, are different manifestations of the same underlying phenomenon, with observed differences being only orientation or obscuration. The main goal of this paper is twofold: (1) to evaluate if the ionized gas in the central regions of LINERs shows characteristics indicative of ionized emission from the AGN (a NLR), and also (2) to investigate their relation to the Seyfert population.

In this paper, we present an update of the properties of the Narrow Line Region for a large sample of 32 LINERs. Archival *HST* narrow imaging data have been used (WFPC2 and ACS). In Section 2 the sample and the *HST* image processing are described. In Section 3 we present the results and discussion. Section 4 summarizes our main conclusions.

2. Sample and data reduction

We have searched for archival *HST* data for the 82 LINERs in our sample (González-Martín et al. 2009a) in the *Hubble Legacy Archive* (HLA hereinafter) web page[1]. HLA data are fully processed (reduced, co-added, cosmic-ray cleaned etc.) images ready for scientific analysis. All the files for narrow band observations centered either in Hα or [O III] emission lines (at the redshift of the galaxy) and their corresponding continuum have been retrieved. For thirty two galaxies, this kind of narrow-band imaging data are available[2]. HLA data products are available for all of them, so we have retrieved the fits files corresponding to averaged, processed data. Table 1 provides the galaxy names (Col. 1), coordinates as provided by HLA (Cols. 2 and 3), instrument (Col. 4; most of the data comes from WFPC2, only 5 galaxies coming from ACS), proposal number and principal investigator's name (Cols. 5 and 6), the filters used in this analisys (Col. 7) and the total exposure time for such filters (Col. 8). The number of images used for each filter is shown in brackets in column 8. When only a single image was available, a cosmic ray extraction was applied by using the LACOSMIC[3] routine (van Dokkum 2001).

HST absolute astrometry does not guarantee the centering of two images at the level of its spatial resolution. For that reason, when needed, the narrow- and wide-band images have been aligned according to the center of the galaxy (maximum peak in brightness) and with the stars present in the field.

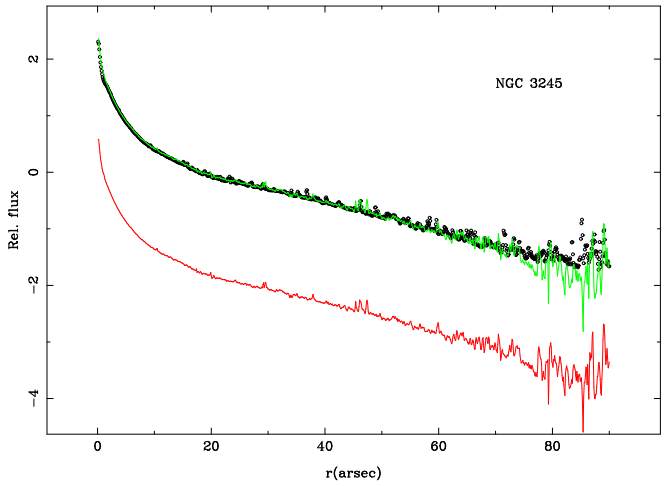

Fig. 1. Surface brightness profiles for NGC 3245. The broad-band profile, $I(F_{wide})$, is plotted in black (circles points). The narrow-band profile, $I(F_{narrow})$, is ploted in red. The green line is the narrow-band profile scaled to that of the broad-band.

In order to maximize the chances to get a reliable estimation of the continuum level at the wavelength corresponding to the emission line, we use a common procedure to get continuum subtracted images, based in a relative calibration as follows. The fluxes in the narrow ($I(F_{narrow})$) and broad band ($I(F_{wide})$) filters are:

$$I(F_{narrow}) = I_{narrow}(cont) + I_{narrow}(line) \quad (1)$$

$$I(F_{wide}) = I_{wide}(cont) \quad (2)$$

where $I_{narrow}(line)$, $I_{narrow}(cont)$, and $I_{wide}(cont)$ are the intensities measured in the line itself, the continuum under the line, and the continuum in the wide filter, respectively.

To assume that line emission is less extended than the continuum is equivalent to say that, far enough from the center, for flux calibrated images one should have $I_{narrow}(cont) = I_{wide}(cont)$. Previous to any calculation, the background of the two images, narrow and wide-band, has been set to zero.

Then, we have to calculate the factor required to put the two images at the same level. To do so, we obtain the surface brightness profiles (with *ellipse* within IRAF[4]) for the narrow- and broad-band images. The comparison of the two profiles allows us both to estimate the region where the fluxes should be fixed at the same level, and then the corresponding factor to be applied. An example of the two profiles obtained for the galaxy NGC 3245 is shown in Fig. 1. The resulting emission-line image is calculated as:

$$I(emission) = I(F_{narrow}) - factor \times I(F_{wide}) \quad (3)$$

The emission line images coming from equation 3 are not flux calibrated, but allow to recover emission-line morphologies and sizes, what is our main purspose, as it will be explained below.

[1] http://hla.stsci.edu/hlaview.html

[2] Also available are the narrow band images of NGC6240 and NGC6241, which are not considered in this paper since the NLR physical sizes for these two galaxies cannot be resolved even with HST data due to their much larger distances.

[3] http://www.astro.yale.edu/dokkum/lacosmic/

[4] IRAF is distributed by the National Optical Astronomy Observatories, which are operated by the Association of Universities for Research in Astronomy (AURA), Inc., under contract with the National Science Foundation.

Table 1. Archival *H*ST data for the LINER galaxies.

Galaxy	Righ Ascension (2000)	Declination (2000)	Instrument	Proposal number	Prop. PI name	Filter	Exposure time (sec)
(1)	(2)	(3)	(4)	(5)	(6)	(7)	(8)
IC1459	22:57:10.607	-36:27:44.00	WFPC2	6537	De Zeew	F631N	2300(3)
						FR680P15	2000(3)
NGC0315	00:57:48.883	+30:21:08.81	WFPC2	6673	Baum	F555W	460(2)
						F814W	460(2)
						FR680N	3300(3)
NGC2639	08:43:38.078	+50:12:20.01	WFPC2	7278	Falcke	F547M	320(2)
				7278	Falcke	F814W	140(2)
				7278	Falcke	FR680P15	1200(2)
NGC2681	08:53:32.730	+51:18:49.30	ACS	9788	Ho	F658N,F814W	720(2),120(1)
NGC2787	09:19:18.560	+69:12:12.00	WFPC2	6785	Malkan	F658N,F702W	2800(4),800(2)
NGC2841	09:22:02.634	+50:58:35.47	ACS	10402	Chandar	F658N,F814W	1400(2),750(2)
NGC3226	10:23:27.008	+19:53:54.68	ACS	9293	Ford	F658N,F814W	1400(2),700(2)
NGC3245	10:27:18.392	+28:30:26.56	WFPC2	7403	Filippenko	F658N,F702W	2200(2),140(1)
NGC3379	10:47:49.600	+12:34:53.90	WFPC2	6731	Ciardullo	F502N,F547M	9785(5),600(5)
NGC3607	11:16:54.660	+18:03:06.50	ACS	9788	Ho	F658N,F814W	700(2),120(1)
NGC3623	11:18:55.960	+13:05:32.00	WFPC2	8591	Richstone	F547M,F658N	1600(4),1600(4)
NGC3627	11:20:15.028	+12:59:29.58	WFPC2	8591	Richstone	F658N	1600(4)
			WFPC2	8597	Regan	F606W	560(2)
NGC3998	11:57:56.133	+55:27:12.91	WFPC2	5924	Dressel	F658N,F791W	1660(3),100(2)
NGC4036	12:01:26.753	+61:53:44.81	WFPC2	5419	Sargent	F547M	300(1)
				6785	Malkan	F658N	2800(4)
NGC4111	12:07:03.130	+43:03:55.40	WFPC2	6785	Malkan	F658N,F702W	1200(2),600(1)
NGC4278	12:20:06.826	+29:16:50.71	WFPC2	6731	Ciardullo	F502N,F547M	12700(5),600(5)
NGC4314	12:22:31.990	+29:53:43.30	WFPC2	8597	Regan	F606W	560(2)
				6265	Jefferys	F658N	600(2)
NGC4374	12:25:03.743	+12:53:13.14	WFPC2	6094	Bower	F547M,F658N	1200(2),2600(2)
						F814W	520(2)
NGC4438	12:27:45.594	+13:00:31.77	WFPC2	6791	Kenney	F656N,F675W	5200(4),1450(4)
NGC4486	12:30:49.423	+12:23:28.04	WFPC2	5122	Ford	F547M,F658N	800(2),2700(2)
NGC4552	12:35:39.807	+12:33:22.83	WFPC2	6099	Faber	F555W,F814W	2400(4),1500(3)
				8686	Goudfrooij	F658N	2300(2)
NGC4579	12:37:43.522	+11:49:05.50	WFPC2	6436	Maoz	F502N,F547M	3200(3),726(5)
						F658N,F791W	1400(2),726(5)
NGC4594	12:39:59.432	-11:37:22.99	WFPC2	5924	Dressel	F658N,F791W	1600(2),100(1)
NGC4636	12:42:49.870	+02:41:16.00	WFPC2	8686	Goudfrooij	F547M	1000(4)
						F814W	400(4)
						FR680P15	2300(2)
NGC4676A	12:46:10.110	+30:43:54.90	WFPC2	8669	Van derMarel	F555W,F814W	320(2),320(2)
						FR680N	1200(2)
NGC4676B	12:46:11.243	+30:43:21.87	WFPC2	8669	Van derMarel	F555W,F814W	320(2),320(2)
						FR680N	1200(2)
NGC4696	12:48:49.276	-41:18:40.04	WFPC2	5956	Sparks	F702W,FR680N	320(2),1200(2)
NGC4736	12:50:53.061	+41:07:13.65	WFPC2	5741	Westphal	F555W	296(3)
				8591	Richstone	F656N	1700(5)
NGC5005	13:10:56.231	+37:03:33.14	WFPC2	6436	Maoz	F502N,F658N	2400(2),1400(2)
						F791W	720(4)
NGC5055	13:15:49.330	+42:01:45.40	WFPC2	8591	Richstone	F547M,F656N	1400(4),1700(5)
NGC5846	15:06:29.286	+01:36:20.24	WFPC2	6357	Jaffe	F702W	1000(2)
				6785	Malkan	F658N	2200(2)
NGC5866	15:06:29.499	+55:45:47.57	ACS	9788	Ho	F658N,F814W	700(2),120(1)

Fig. 2 shows the resulting continuum subtracted images for all the galaxies listed in Tab. 1. Both Hα and [O III] images are shown when available (for NGC 4579 and NGC 3379). Overlaid to the grey scale images a number of contours are shown, the faintest corresponding to 3 times the dispersion of the background, σ.

Fig. 2 also shows the sharp divided continuum images (SD hereinafter). Briefly, the sharp-dividing method consists on dividing the original image by another one that results from applying a filter to the original image, with a box size several times that of the PSF FWHM. In our case, a median box of 30 pixels has been used. SD images provide an enhancement of the small structures and thus will be in many cases a good tracer of the dust structures (see Marquez et al. 2003 and references therein), as it is the case, for instance, for NGC 4374 (see Fig. 2).

Appendix A gives a description on the morphology for each object together with additional relevant information.

For estimating the sizes of the emission-line regions, we consider a 3σ level above the background and measure the area of the region inside the corresponding contour. The size is parametrized as the equivalent radius of such an area, i.e.: $R_{eq} = (Area/\pi)^{1/2}$. The σ of the background level for each image has been measured in several regions around the galaxy, so that the final R_{eq} is the median of these values, and its accuracy is provided by the dispersion of the various R_{eq} around the median. The results are presented in Table 2. No radius has been determined neither for NGC 3379 due to low S/N of the images, nor for NGC 3627 and NGC 5866 due to the large amount of dust wich difficults their determination. Col. 1 shows the galaxy name, Col. 2 the filter used for continuum substraction, Col. 3 the distance as taken from González-Martín et al. (2009a), Cols.

4 and 5 show the X-ray soft and hard luminosities taken from Gonzalez-Martín et al. (2009a)[5] and Cols. 6 and 7 the equivalent radius and its dispersion, σ_{Req}. Two estimates of the equivalent radius have been obtained when two continuum filters were available. The deepest resulting image has been chosen to estimate the final equivalent radius. In these cases, the corresponding filter is flagged with an asterisk (in Col. 2). This estimation can be compared with sizes from other analysis based on 3σ detection limits for the extended emission (see for instance Schmitt et al. 2003)

Nevertheless, since the data are inhomogeneous, a S/N threshold does not have a well defined physical meaning, which complicates the interpretation of equivalent radius. Therefore, we have used the flux calibration corresponding to the images taken with narrow band filters, $I(F_{narrow})$ (done in the standard way, using the information available on the image headers), for the resulting emission-line image, once the continuum is rescaled and subtracted, $I(emission)$. Due to the uncertainties in the flux calibration for ramp filters, the images obtained with such filters have not been used. For the flux calibrated images, we have also calculated R^*_{eq} (Col. 8 in Table 2) as the isophotal equivalent radius at the isophotal level of 2.9×10^{-9} erg s^{-1}cm^{-2} arcsec^{-2}. This rather arbitrary surface brightness was chosen to optimize the measure for all the available data. This radius allows a measure of a physical characteristic size of the regions independently on the individual S/N ratios of the images. This has been done for the 22 objects with flux calibrated images.

3. Results and discussion

3.1. Hα emission as a tracer of the morphology of the NLR in LINERs

The first result from our analysis is that for most LINERs the Hα emission is composed of a nuclear source and extended emission, revealing a complex structure, with a large range of different morphologies. The exceptions are NGC 2639, NGC 3379, NGC 3627, NGC 4036 and NGC 5005, for wich an unresolved nuclear source has not been identified. We have grouped our sample galaxies into 4 types of objects according to the morphology of the extended Hα emission in the central 1-2 arcseconds. The objects belonging to each sub-cathegory are shown in Table 3.

1. *Core-halo:* When a clear unresolved nuclear source, surrounded by diffuse emission, has been identified. Nine out of the 32 objects belong to this class. In most cases the putative nucleus is sitting in a linear elongated structure. In five cases (IC 1459, NGC 315, NGC 2639, NGC 3623, and NGC 5055; see individual comments in Appendix A) the extended emission appears to be sitting in the disk of the galaxy and the elongation of the emission follows the major axis of the galaxy (taken from the NED database[6]). In three of them (NGC 2787, NGC 3998, and NGC 4111), the nuclear disk axis seems to be perpendicular to the galaxy major axis. NGC 2681 does not show any elongation (see Fig. 2).
2. *Outflows:* Eleven galaxies show morphological evidences to have nuclear outflows (Veilleux et al 2005). Some of them present debris/filamentary extension (NGC 4486, NGC 4676A and B, NGC 4696, NGC 5005, and NGC 5846), biconical structures (NGC 4036 and NGC 5005) and also buble-like structures (NGC 3245 and NGC 4438) coming out from the nucleus. The high spatial and spectral resolution spectroscopic data (*HST-STIS*) for NGC 3245, NGC 4036 and NGC 4579, reported by Walsh et al. (2008), indeed evidence outflow kinematics strengthening our suggestion. For the remaining objects, such a kinematical confirmation has to await until similar spectroscopic data are available.
3. *Disky:* Seven galaxies present face-on structures that can be associated to Hα emission along the spiral arms (NGC 2681, NGC 2841 and NGC 4736), diffuse emission along the disk (NGC 3379, NGC 4552 and NGC 4636), nuclear plus star formation rings (NGC 4314). NGC 4594 has also been included in this class because, although it is not seen face on, it appears that its Hα emission is concentrated in the nuclear region and their spiral arms.
4. *Dusty:* Those where clear dust lanes obscure the underlying Hα structure. This prevents us from getting information on the morphology of these inner regions. Five objects have been classified as such (NGC3226, NGC3607, NGC3627, NGC4374 and NGC5866). Different structures can be identified depending on the dust distribution along the galaxy, but mostly nuclear sources surrounded by an inhomogeneous dusty disk are found.

Table 3. Morphological classification of Hα nuclear emission.

core-halo	outflow	dusty	disky
IC 1459	NGC 3245	NGC 3226	NGC 2681
NGC 315	NGC 4036	NGC 3607	NGC 2841
NGC 2639	NGC 4438	NGC 3627	NGC 3379
NGC 2787	NGC 4486	NGC 4374	NGC 4314
NGC 3623	NGC 4579	NGC 5866	NGC 4552
NGC 3998	NGC 4636		NGC 4594
NGC 4111	NGC 4676A		NGC 4736
NGC 4278	NGC 4676B		
NGC 5055	NGC 4696		
	NGC 5005		
	NGC 5846		

Our main concern here is to understand whether the detected Hα nuclear regions correspond to the expected NLR for AGN. Pogge et al. (2000) made an extensive *HST* investigation on the NLR of 14 LINERs, and concluded that at *H*ST resolution the NLRs are resolved showing complex morphologies, different from galaxy to galaxy, that come from a combination of knots, filaments and diffuse gas. Dai & Wang (2008) concluded similarly with an extension of Pogge's sample up to 19 LINERs.

Among our 32 sample galaxies, 17 LINERs are studied in this paper for the first time. Pogge et al. (2000) already analized 7 of the LINERs in our sample (namely NGC 3998, NGC 4036, NGC 4374, NGC 4486, NGC 4579, NGC 4594 and NGC 5005) and Dai & Wang (2008) studied another 4 (namely NGC 404, NGC 2768, NGC 3718 and NGC 4192) not included in the sample because of our X-ray selection.

All together, including the new 17 LINERs from our work plus the 19 ones from Dai & Wang (2007) (we have 15 objects in common with them), they conform a rather homogeneous set of data for 36 LINERs, which seems to be the larger sample homogeneously analyzed so far. It is worth noticing that the 4 objects from Dai & Wang's paper not included in our sample can be fit into the outflow-like group. Thus from the total sample of 36 LINERs, 42 % would be outflow candidates, 25% core-halo systems, 19% disk-like systems and 14% dusty LINERs. These

[5] The L_X (2-10 keV) are Compton-thick corrected.

[6] The NASA/IPAC Extragalactic Database (NED) is operated by the Jet Propulsion Laboratory, California Institute of Technology, under contract with the National Aeronautics and Space Administration.

Table 2. X-ray luminosities[a] and Hα equivalent radii[b].

Galaxy	Cont. Filter	D[a]	log(L^b_{soft})	log(L^b_{hard})	R^c_{eq}	σ_{Req}	R^{*c}_{eq}
		(Mpc)	(erg/s)	(erg/s)	(pc)	(pc)	(pc)
(1)	(2)	(3)	(4)	(5)	(6)	(7)	(8)
IC 1459	FR680P15	29.24	40.6	40.5	245.52	0.17	
NGC315	F555W	68.11	42.0	41.8	398.66	0.02	
	F814W*	68.11	42.0	41.8	528.32	0.22	
NGC2639	F547M*	45.45	42.2	40.1	212.37	0.18	
	F814W	45.45	42.2	40.1	185.79	0.12	
NGC2681	F814W	17.22	38.6	41.0	209.75	0.07	48.27
NGC2787	F702W	7.48	38.9	38.8	43.50	0.03	29.11
NGC2841	F435W*	11.97	39.4	39.2	167.91	0.02	
	F814W	11.97	39.4	39.2	142.97	0.25	16.36[d]
NGC3226	F814W	23.55	40.7	40.8	100.49	0.02	29.53[d]
NGC3245	F702W	20.89	38.8	40.8	117.78	0.21	158.90
NGC3379	F547M	10.57	38.0	39.9			
NGC3607	F814W	22.80	38.6	40.5	283.65	0.31	27.17[d]
NGC3623	F547M	7.28	39.1	39.4	86.33	0.08	35.52
NGC3627	F606W	10.28	39.2	41.2		0.08	109.45
NGC3998	F791W	21.98	42.7	40.6	237.93	0.08	233.01
NGC4036	F547M	24.55	39.0	40.9	199.21	0.06	116.29
NGC4111	F702W	15.00	40.9	40.4	132.19	0.03	308.69
NGC4278	F814W	16.07	39.6	41.0	67.0	0.08	118.34
NGC4314	F606W	9.68	39.6	39.1	165.01	0.04	
NGC4374	F547M	18.37	39.5	41.3	401.75	0.03	
	F814W*	18.37	39.5	41.3	340.93	0.06	197.53
NGC4438	F675W	16.83	40.1	40.8	255.57	0.02	153.53
NGC4486	F547M	16.07	40.9	40.8	224.74	0.08	81.99
NGC4552	F814W	15.35	39.5	39.3	216.95	0.15	217.22
NGC4579	F791W	16.83	40.9	41.2	145.98	0.03	174.22
	F547M	16.83	40.9	41.2	45.09	0.01	
NGC4594	F791W	9.77	39.6	39.9	93.35	0.09	107.34
NGC4636	F814W	14.66	39.0	40.9	54.75		
NGC4676A	F555W*	88.00	39.7	39.9	598.38	0.10	
	F814W	88.00	39.7	39.9	769.16	0.06	
NGC4676B	F555W*	88.00	40.0	40.1	1001.37	0.06	
	F814W	88.00	40.0	40.1	843.25	0.05	
NGC4696	F702W	35.48	41.6	40.0	205.77	0.15	
NGC4736	F555W*	5.20	38.8	38.6	146.49	0.03	
	F814W	5.20	38.8	38.6	252.39	0.01	226.27
NGC5005	F791W	21.28	40.7	41.6	248.99	0.03	393.56
NGC5055	F547M	7.14	38.6	39.6	76.04	0.06	62.92
NGC5846	F702W	24.89	40.2	40.8	156.31	0.08	88.26
NGC5866	F814W	15.35	40.1	38.1			

[a] Distances have been taken from table 1 in González-Martín et al. (2009a)
[b] Note that these luminosities have been corrected from intrinsic absorption; L_X (2-10 keV) has been also corrected for Compton-thickness. L_{hard} and L_{soft} hold for the logarithm of the (2-10) kev (from Gonzalez-Martín et al. 2009b) and (0.3-2) keV (from Gonzalez-Martín et al. 2009a)
[c] R_{eq} is the equivalent radius corresponding to a level 3 times higher that the dispersion of the background. R^*_{eq} corresponds to the isophotal level at 2.9×10^{-9} erg s^{-1}cm^{-2} arcsec^{-2}.
[d] The resulting radius is smaller than 2 pixels.

results stress the intereresting possibility of shock heating as an extra contribution to the ionization in addition to nuclear photoionization. This scenario needs to be explored at length with high S/N spectroscopy for the outflow candidates to investigate if at least for these LINERs the long standing problem of ionizing-photon deficit can be solved (see Eracleous et al. 2010b for a full discussion).

The question then to be answered is whether the origin of the outflow can be circumnuclear star formation or it is a nuclear outflow predicted by the unified AGN models (Elvis 2000). From the STIS spectroscopic analysis by González Delgado et al. (2004) it is found that recent star forming processes (with ages lower than 10^7 years) are almost absent in LINERs, being the dominant stellar population that of old stars with, in some particular cases, some contribution from intermediate age (10^8 years) stars. The Hα identified structures appear to be consistent with such a picture. Indeed, at the HST resolution of few tens of parsecs, a knotty appearance should be expected when young star clusters are present, which is not observed in most of the images. Their inspection appears to indicate that such knotty structures are only present in the Mice system. In disk-like systems, star formation can be distinguished in their disks (e.g. see the star formation ring on NGC 4314 at ∼200 parsecs from the nucleus, Fig. 2). The structure of core-halo galaxies is more likely originated from the gas ionized by the nucleus. For dusty galaxies, although a faint nuclear source is visible in most of them, the dust distribution prevents us from drawing any conclusion on the extended ionized gas.

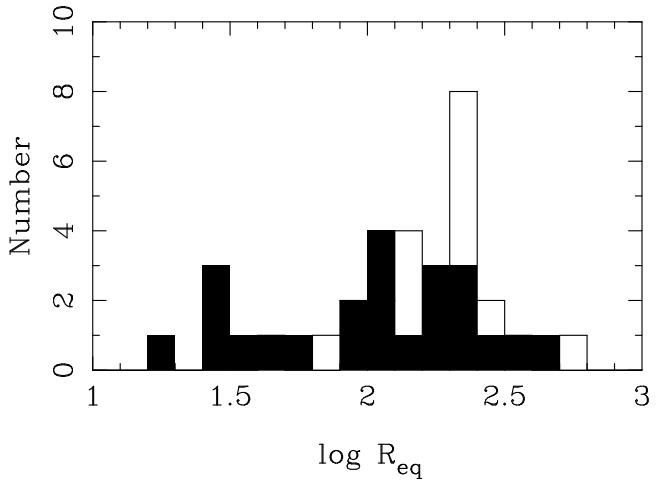

Fig. 3. Histograms of equivalent radii R_{eq} (in parsecs),in our LINER sample. The black filled area shows the R^*_{eq} distribution.

3.2. Quantification of the Hα emission: equivalent radius

To further investigate the origin of the extended Hα emission, and considering its irregularity, we have calculated a characteristic radius for estimating the size of the ionized region: the equivalent radius, R_{eq}, and R^*_{eq} provided in Table 2[7] (see Section 2, for a detailed explanation of the methodology).

We searched for a distance dependence that could bias our result, so we plotted equivalent radii in arcseconds *versus* distance and did not found any correlation between the two quantities. In Fig. 3 the distribution of R_{eq} in parsecs is shown as the empty histogram and the corresponding R^*_{eq} distribution as the black filled area. A range of values between 43 and 528 pc with a median value of 200 pc has been obtained for R_{eq} and between 16 and 469 pc, with a median value of 116 pc for R^*_{eq}. Comparing both estimations, it is found that with the exception of NGC 4111, NGC 4314 and NGC 5005 for which it is found the largest values of R^*_{eq} and much smaller values from the R_{eq} estimation , for the remaining cases R^*_{eq} is equal or lower than R_{eq}. Thus we can conclude that the currently more extended used size estimation at 3σ detection limits tend to overestimate the true physical size of the nebula. Finally it is worth to note that no significative difference is found on the size among the different morphologies.

This range of values is similar to that reported by Dai & Wang (2008). For the 14 galaxies with measured radii in common in both works, our estimations for NGC 2787, NGC 4111, and NGC 4594 are smaller; large discrepancies are found for three objects (for NGC 4314 and NGC 4736 Dai & Wang measured very small values and for NGC 4374 a rather large value was measured compared to ours); for the remaining ten objects our estimations are larger than theirs. We stress that the method used by Dai & Wang (2008) relies on the estimation of the annulus at which the 3-σ level above the continuum is reached (see also Bennert et al. 2002). The general irregularity of the isophotes makes this method rather uncertain, what has motivated us to use R_{eq}, that we consider a more realistic estimation of the size of the emitting regions.

Our sizes cover the lower end of the distribution of values for the major axis obtained, with [OIII]-HST imaging (Schmitt et al. 2003) for the NLR of Seyfert galaxies. For the 10 Seyfert galaxies with HST data from Schmitt et al.'s sample included in the X-ray catalog CAIXA[8], we have recalculated the sizes using our definition of R_{eq} and obtained a range of values between 56 and 314 pc with a median of 169 pc, very much the same than the value for LINERs. Althought the comparison is not straightforward since for Seyferts most of the data comes from the [OIII] line, it is however very suggestive that their NLR morphologies and sizes are not very different from those of LINERs.

3.3. Luminosity - size relation

The luminosity - size relation can also be used to get insight onto the nature of the ionized emission. This has been raised as an important relation for AGN since Peterson et al. (2002) found that it can be defined for the BLR of Seyferts. Greene et al (2010) have revisited such a dependence and found that it is consistent with $R_{BLR} \propto \sqrt{L}$ based both in Balmer lines and hard (2-10 keV) luminosities. This is the expected dependence when the BLR density is independent on luminosity. Their data also suggest a steeper relation for the narrow line luminosities, $R_{BLR} \propto L^{0.6}$.

Bennert et al. (2002) and Schmitt et al. (2003) searched for such a relation for the NLR of Seyferts and Dai & Wang (2008) extended the work to LINERs. They concluded that LINERs follow the same relation than Seyferts and QSOs. In this work we present this relation, but for the first time using the X-ray luminosity instead of that of Hα, which is a more robust tracer of the power of the AGN (Maiolino et al. 2002). Hα is expected to be more contaminated by other processes as recent star formation events.

The X-ray luminosity can be used as a measure of the bolometric intrinsic luminosity of an AGN (Gonzalez-Martín et al 2006, 2009a and b). Therefore, it is worthwhile to investigate whether it is related to the size of the NLR. In Fig. 4 the hard (2-10 keV) X-ray luminosity *versus* the two determinations of the equivalent radius is presented. The different Hα morphologies described in Section 3.2 are plotted with different symbols. The following three galaxies have been excluded from the plot: NGC 3379, NGC 3627 and NGC 5866. NGC 3379 was excluded because the low count rates of its narrow line image impede the determination of a reliable equivalent radius; NGC 3627 and NGC 5866 were excluded because large amounts of dust hampers the detection of their NLR. The two galaxies conforming the Mice system (NGC 4676A and NGC4676B) show a large knotty extension of star formation regions together with typical structures of outflowing material, leading to a rather large value of equivalent radius exceding the hypothetical NLR. Therefore, despite their inclusion in the plots, they won't be used for any correlation below.

A first attemp to look for a correlation between X-ray luminosities and R_{eq} is based on a least square linear fit, that results in the values reported in Tab. 4, and not plotted in Fig. 4 for clarity. The correlations are quite bad, with all the galaxies classified as disky (but NGC 4594) showing larger sizes than those expected from their luminosities for the remaining galaxies. This is not unexpected, since $H\alpha$ emission in disky galaxies also comes from the contribution of ionized regions in their disk. Therefore we tried again a linear fit, but this time excluding disky galaxies. The result is the full line in Fig. 4. The resulting coefficients imply better correlations in this case (see Tab. 4). Finally, we fitted

[7] Radii smaller than 2 pixels, identified with [c] in Column 7, are not considered.

[8] Catalog of AGB in the XMM-Newton archive, Bianchi et al. (2009).

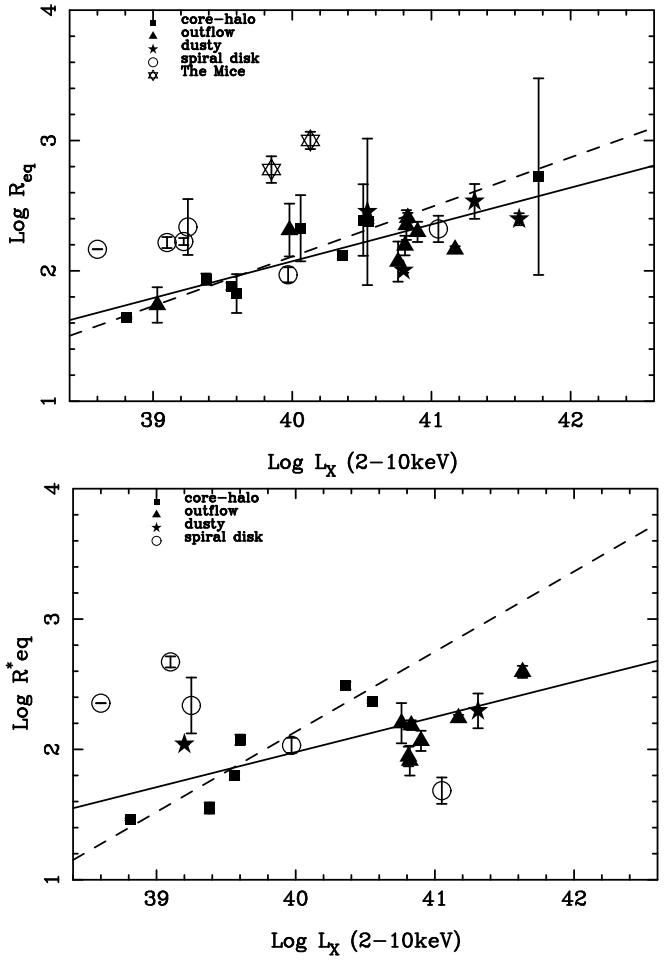

Fig. 4. Top: (2-10) keV band absorption corrected luminosity versus the equivalent radius to the contour corresponding to 3σ times the background, R_{eq}. Bottom: The same for the equivalent radius of the level corresponding to 2.9×10^{-9} erg s^{-1}cm^{-2} arcsec^{-2}, R^*_{eq}. The equivalent radii are derived thought narrow band *HST* images. The full lines show the best linear fit to all the galaxies excluding disky systems. The dashed lines show the best linear fit to the core-halo systems.

just the core-halo systems (dashed line in Fig. 4), resulting in the best correlation (see Tab. 4).

Therefore, two main results appear from Tab. 4: (1) The luminosity-size relation is better when using X-ray luminosities at harder energies and (2) a better correlation is found when disky systems are excluded from the fitting, the best fit resulting when only core-halo systems are taken into account.

This later result can be due to the fact that core-halo systems appear to be less dusty and therefore provide a clear insight on the NLR. Since the hard X-ray luminosities cannot be produced by stars, this relation support the nature of the emission regions as the result of the ionization by the AGN. In that respect it is very suggestive of the similarity of LINERs with higher power AGN, that the slope for core-halo systems (0.38) has the same value than that reported for Seyfert galaxies by Schmitt et al. (2003) by using the [O III] luminosity as a proxy of the AGN power.

The resulting correlations for the subset of calibrated data are shown in Fig. 4 (bottom) and in Tab. 4. It is very interesting to notice that a significant correlation remains only for the core-halo systems. Both dusty and outflow galaxies appear to have lower equivalent radii for their X-ray luminosities. For the dusty systems it is obvious that the presence of large amounts of dust obscures the inner regions and thus lowers the measured size of the Hα emission. The explanation for the outflow candidates is not so straightforward. It appears that they cover a narrow range on X-ray luminosities. This result may suggest a different origin for the emission mechanism in these systems but needs to be further investigated.

3.4. Soft X-rays vs NLR morphologies

For a collection of 8 Seyferts, Bianchi et al. (2006) have reported a spatial correlation between the soft X-ray emission and the NLR as reflected by the [OIII] emission, taking this result as an important evidence on the photoionized nature of soft X-rays. Given the morphological similarity between the NLR of Seyferts and LINERs (Schmitt et al 2003, Pogge et al 2000), it will be interesting to explore if such a relation does exist also in LINERs.

In Fig. 6 the soft X-ray isocontours are overploted (in black) over the Hα images. Only the 28 galaxies with available Chandra imaging have been included. The remaining 4 galaxies have only XMM-Newton X-ray data, as indicated in Table 5 with an asterisk in Col. (6). Althought a very detailed comparison cannot be made due to the different resolutions at both wavelenghts (around 1" and 0.1" for Chandra and HST data, respectively) it is remarkable that soft X-rays and Hα data show a rough coincidence in their shapes, the soft X-ray contours following the structures identified with HST. This is not the case for the hard X-rays (red contours in Fig. 6). Few galaxies depart from the general behaviour, NGC 3226, NGC4486, NGC 4676A and B, NGC 5846 and NGC 5866. NGC 3226 show a compact structure both at soft and hard X-rays, whereas the Hα distribution seems to suggest an outflow coming out from that compact nucleus. For NGC 4486, both soft and hard X-rays follow the radio jet also visible in the continuum images, being the Hα outflow perpendicular to it. NGC 4676A and B and NGC 5846 shows in Hα a structure non-coincident with either hard or soft X-rays, suggesting that the emitting gas has a different origin. No conclusion can be obtained for NGC 5866: its Hα emission appear to be very obscured by large amounts of dust and soft X-rays show a spatial distribution which appears to be out of the plane of the galaxy.

Unfortunatelly there does not exist yet a sample of good RGS XMM-Newton data for LINERs to allow the modelling of the soft X-ray emission. However the data reported by Starling et al. (2005) on the LINER galaxy NGC 7213 and those collected for 53 LINERs by González-Martín et al. (2010, in preparation) seem to suggest that their soft emission comes from photoionized gas, in good agreement with the conclusions obtained with the systematic work on Seyfert 2 galaxies by Bianchi and colaborators (Bianchi et al. 2006, Bianchi et al. 2010).

3.5. Multiwavelength properties

Different authors (Ho et al. 1999; Maoz 2007; Eracleous et al. 2009, 2010a; González-Martín et al. 2009a) have recognized the importance of the multiwavelenght information to get a clear picture of the enegy source in LINERs. Table 5 shows relevant information for the LINERs in this sample. The information in Cols. from (2) to (10) has been extracted from Tab. 12 in González-Martín et al. (2009a), with Col. (1) providing their number code for each galaxy. In Col. (6) the word CT has been added when a LINER shows Compton-thick (CT hereinafter)

Table 4. Fitting parameters for the correlations between the equivalent radius and X-ray luminosity.

		R_{eq}		R^*_{eq}	
	energies	slope	Correl. coeff.	slope	Correl. coeff.
full sample	(2-10keV)	0.179 ± 0.044	0.630	0.069±0.082	0.193
	(0.5-2 keV)	0.056 ± 0.040	0.266	0.114±0.064	0.389
non-disklike	(2-10keV)	0.282 ± 0.054	0.814	0.269 ±0.070	0.727
	(0.5-2 keV)	0.074 ± 0.049	0.324	0.144 ±0.064	0.530
core-halo	(2-10keV)	0.380 ± 0.047	0.949	0.615±0.116	0.936
	(0.5-2 keV)	0.173 ± 0.056	0.757	0.221±0.073	0.834

characteristics as defined in González-Martín et al. (2009b). Col. (7) has been updated with the corresponding references for three objects. Col. (9) gives the final classification considering the multiwavelength information from Cols. (3) to (8). Col. (10) provides the HST morphological class as defined in this paper. In Col. (11) we present the Eddington ratio, R_{Edd}, calculated using the formulation given in Eracleous et al. (2010a):

$$R_{Edd} = 7.7 \text{ x } 10^{-7} \text{ } L_{40} \text{ } M_8{}^{-1}$$

where L_{40} is the bolometric luminosity in units of 10^{40} erg s^{-1} and M_8 is the black hole mass in units of 10^8 $M_\odot$. The SED obtained by Eracleous et al (2010) for LINERs leads to a bolometric luminosity 50 times $L_{2-10keV}$. Both $L_{2-10keV}$ and M_8 values have been taken from Gonzalez-Martín et al (2009b).

As we did in Sect. 3.2., the two components of the Mice system will not be included in the discussion; their rather complex nature resulting from the merger-like interaction between NGC 4676A and B, is unique among our sample galaxies and may contaminate our results. Our discussion will therefore be dealing with the remaining 30 galaxies.

From the 4 LINERs with a final classification as non-AGNs according to Col. (9), NGC 3623 has an uncertain X-ray classification since it is based in XMM-Newton data. The other 3 (namely NGC 3379, NGC 4314 and NGC 4278) show an Hα classification as disk-like systems. Their X-ray data show evidences to be Compton-thick (Gonzalez-Martín et al 2009b), what suggests that they could well host extremely obscured AGN activity.

For 3 out of the 26 confirmed AGN LINERs (namely NGC 3607, NGC 3627 and NGC 5866), their classification is only based on the detection of a broad Hα line, being classified at X-rays as non-AGNs. They all have an HST classification as dusty objects and appear to be Compton thick at X-ray frequencies, so in these three cases a hint of a relationship between the obscuring materials could be claimed.

In addition to these, 10 more AGN LINERs show evidences of CT nature. In 5 of them (namely NGC 2639, NGC 4374, NGC 4552, N4636 and NGC 5846) BLRs have been detected. Only a dusty environment is seen with the HST data for NGC 4374. For the other 4 galaxies the obscuring material seems to be most probably sitting in the innermost regions. Seven out of the 13 CT LINERs show their BLR, among which 4 of them have dusty Hα morphologies. Therefore, for the remaining 3 out of the 7 CT LINERs there is no obscuring material at HST resolution that could be invoked as the origin of its CT nature. A similar result has been found for Seyferts 1 (Malizia et al. 2009, Panessa et al. 2008), questioning the dichotomy type 1/type 2 AGNs in the current unification models (Urry and Padovani 2000). Finally for the remaining CT narrow-line LINERs (NGC 2681, NGC 3245, NGC 4036, NGC 4438, NGC 5005 and NGC 5055) the obscuration cannot be atributed to important dust lanes obscuring the nuclei. Summarizing the results on CT LINERs, a large incidence is found in the dusty systems, since 4 out of the 5 dusty systems are CT; the remaining are distributed among the different types.

Althought the number statistics are rather low, it is very interesting to notice that among secured X-ray AGN-classed LINERs, based on Chandra observations, (19 out of 24 galaxies, see Col. (6) in Tab. 5) outflow and core-halo morphologies prevail (6 outflow systems, 7 core-halo, 4 disk-like and 2 dusty) amounting to 68%. Taking the 26 galaxies AGN-classed based on multifrequency data, 8 have been classified as core-halo, 9 as outflow, 4 as disky and 5 as dusty. Therefore outflows and core-halo represent 65% of the AGNs.

Considering the Eddington ratios, the large range obtained (from 10^{-7} to 10^{-2}) overlaps with the values found for Seyfert galaxies (Panessa et al. 2006, Gonzalez-Martín et al 2009a), suggesting that LINERs are not always the low accretion cousins of Seyferts. We have found a slight trend for the Eddington ratios to decrease when moving from core-halo to outflow and disky systems (see Fig. 5). Dusty galaxies are not considered in the general trend since in the absence of dust they should fit in one of the other 3 classes. Different authors have claimed that strong radio jets are responsible for the bulk of the radio emission observed in LINERs (Nagar et al. 2005, Filho et al. 2002) and that the radio loudness parameter (see Maoz 2007) can be related to the Eddington ratios in the sense that Eddington ratios are larger for lower radio loudness ratios. Maoz (2007) speculate that, in order to explain high Eddington ratios in low luminosity AGNs, mechanisms preventing gas to reach the inner parts of the accretion disk would be at work; they suggest radio loudness at low luminosities as such a solution, with the gas joining a jet or an outflow. Our data seem to support such a hypothesis since 1) radio loud systems are found in core-halo and outflow systems and, even more important, 2) all the outflow systems appear to be radio-loud.

4. Summary and conclusions

We have presented HST-Hα imaging of 32 LINERs, selected from the X-ray sample studied in our previous works (González-Martín et al. 2009a and b). A full description of the extraction and reduction process is given and the resulting emission-line images are also presented together with the sharp divided continuum images for each galaxy. The description of the most relevant properties for each individual galaxy is also given.

The main conclusion from this analysis is that, for the large majority of LINERs, an unresolved nuclear source has been identified, together with extended emission with equivalent sizes ranging from few tens of parsecs till about 500 pc. Adding up additional 4 LINERs from the literature to our sample, we conclude that their emission-line morphologies appear not to be homogeneous, being basically grouped into three classes: nuclear outflow candidates (42%), core-halo morphologies (25%) and

Table 5. Multiwavelength properties of LINERs.

Num	Name	UV Var.	X-ray Var.	UV Comp.	X-ray Class.	Radio Comp.	Broad Hα	Final Class	*HST* Class.	R_{Edd}
(1)	(2)	(3)	(4)	(5)	(6)	(7)	(8)	(9)	(10)	(11)
80	IC 1459				AGN		Y	Y	core-halo	$5.0x10^{-5}$
1	NGC 0315				AGN	Y	Y	Y	core-halo	$1.0x10^{-3}$
9	NGC 2639				Non-AGN* CT	Y	Y	Y	core-halo	$7.9x10^{-3}$
11	NGC 2681			Y	AGN CT	Y	N	Y	core-halo	$3.2x10^{-5}$
15	NGC 2787			N	AGN	Y	Y	Y	core-halo	$2.5x10^{-6}$
16	NGC 2841				AGN			Y	disky	$6.3x10^{-6}$
19	NGC 3226				AGN	Y	Y	Y	dusty	$1.3x10^{-4}$
20	NGC 3245				AGN CT	Y[a]	N	Y	outflow	$1.0x10^{-6}$
21	NGC 3379				Non-AGN CT		N	N	disky	$2.0x10^{-7}$
24	NGC 3607				Non-AGN CT		Y	Y	dusty	$5.0x10^{-7}$
26	NGC 3623				Non-AGN*		N	N*	core-halo	$1.2x10^{-5}$
27	NGC 3627				Non-AGN* CT		Y	Y	dusty	$7.9x10^{-6}$
32	NGC 3998	Y	Y	Y	AGN	Y	Y	Y	core-halo	$2.5x10^{-3}$
33	NGC 4036				AGN CT	Y	N	Y	outflow	$3.2x10^{-6}$
34	NGC 4111			N	AGN		N	Y	core-halo	$7.9x10^{-4}$
39	NGC 4314			N	Non-AGN CT		N	N	disky	$1.0x10^{-4}$
39	NGC 4278			N	Non-AGN CT		N	N	disky	$1.2x10^{-4}$
41	NGC 4374				AGN CT		Y	Y	dusty	$1.6x10^{-6}$
43	NGC 4438			N	AGN CT	Y	N	Y	outflow	$6.3x10^{-5}$
46	NGC 4486	Y	Y	Y	AGN	Y	Y	Y	outflow	$2.5x10^{-5}$
48	NGC 4552	Y	Y	Y	AGN		Y	Y	disky	$3.9x10^{-6}$
50	NGC 4579	Y	Y	Y	AGN	Y	Y	Y	outflow	$2.5x10^{-4}$
52	NGC 4594	Y		Y	AGN		Y	Y	disky	$3.9x10^{-6}$
53	NGC 4636				Non-AGN CT	Y	Y	Y	outflow	$2.1x10^{-6}$
54	NGC 4676A				Non-AGN			N	outflow	...[b]
55	NGC 4676B				AGN			Y	outflow	$6.3x10^{-6}$
57	NGC 4696				Non-AGN	Y[c]	Y	Y	outflow	$3.9x10^{-4}$
58	NGC 4736	Y		Y	AGN		Y	Y	disky	$1.0x10^{-5}$
59	NGC 5005		Y		AGN* CT?	Y	N	Y	outflow	$1.0x10^{-5}$
60	NGC 5055			Y	AGN CT		N	Y	core-halo	$1.0x10^{-5}$
70	NGC 5846				Non-AGN CT	Y[c]	Y	Y	outflow	$2.0x10^{-5}$
71	NGC 5866				Non-AGN CT		Y	Y	dusty	$5.0x10^{-5}$

[a] From Wu & Cao (2005)
[b] No BH mass is available for this source
[c] From Dunn et al. (2010)

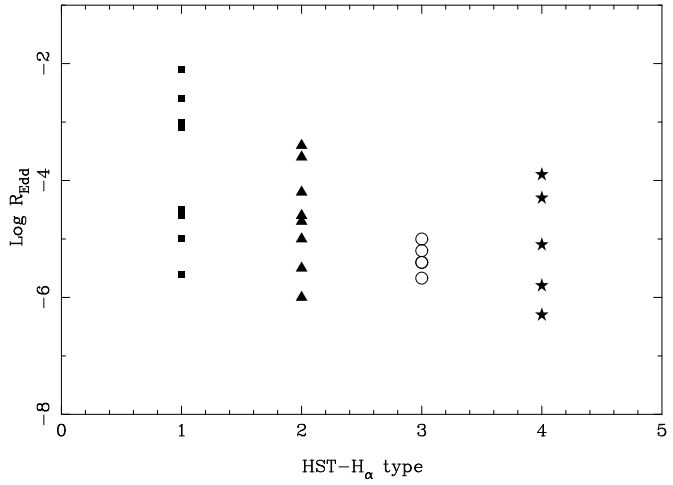

Fig. 5. Eddington ratios as a function of the HST-Hα classification for the AGN LINERs in our sample. Symbols are the same as in Fig. 4.

nuclear spiral disks (14%), being the remaining 5 galaxies too dusty to allow a clear view of the ionized distribution. Except maybe for the only case of a merger-like interaction (the two galaxies in the Mice system), no signatures of clumpy structures reminiscent of star clusters have been identified, in agreement with results from stellar population analisis (González-Delgado et al. 2004 and Sarzi et al. 2006).

A size-luminosity relation has been found between the equivalent radius of the Hα emission and the hard X-ray luminosity. This correlation ressembles that reported for the NLR of Seyferts galaxies based in the [OIII] luminosity (Schmitt et al. 2003). This relation is another piece of evidence confirming the AGN-NLR nature of the ionized gas in LINERs (Pogge et al. 2000, Walsh et al. 2008).

Indications of a relationship between soft X-rays and Hα emission in LINERs are also reported for the first time. This spatial correlation looks similar to the one reported by Bianchi et al (2006) for Seyferts, evidencing the photoionized nature of the soft X-rays.

For the only 4 LINERs with no evidences for AGN nature of their nuclear emission, a CT AGN cannot be discarded out given the properties of their X-ray emission. For the confirmed AGN-LINERs, their Hα morphologies favour core-halo and outflow systems (65% of the cases). Finally, Eddington ratios have been calculated showing that LINER nuclei radiate in the sub-

Eddington regime, in agreement with previous data (Maoz 2007, Ho 2008, Eracleous et al. 2010a). However core-halo systems tend to have larger Eddington ratios than outflow candidates on average. These result may be consistent with the suggestion by Maoz (2007) of radio-loud outflow related systems showing smaller Eddington ratios.

Acknowledgements. J.M. and I.M. acknowledge financial support from the Spanish grant AYA2007-62190 and Junta de Andalucía TIC114 and the Excellence Project P08-TIC-03531. O.G-M acknowledges finantial support by the EU FP7-REGPOT 206469 and ToK 39965 grants. A.R. acknowledge finantial support from CONACyT grant number +081535. We acknowledge the valuable feedback from an anonymous referee. Based on observations made with the NASA/ESA Hubble Space Telescope, and obtained from the Hubble Legacy Archive (HLA hereinafter), which is a collaboration between the Space Telescope Science Institute (STScI/NASA), the Space Telescope European Coordinating Facility (ST-ECF/ESA) and the Canadian Astronomy Data Centre (CADC/NRC/CSA). This research has made use of the NASA/IPAC Extragalactic Database (NED) which is operated by the Jet Propulsion Laboratory, California Institute of Technology, under contract with the National Aeronautics and Space Administration.

References

Barth, A. J., Ho, L. C., Filippenko, A. V., & Sargent, W. L. W. 1998, ApJ, 496, 133
Barth, A. J., 2002, ASP Conf. Ser. vol. 258, 147
Bennert, N., Falcke, H., Schulz, H., Wilson, A. S., & Wills, B. J. 2002, ApJ, 574, L105
Bianchi, S., Guainazzi, M., & Chiaberge, M. 2006, A&A, 448, 499
Bianchi, S., Guainazzi, M. Matt, G. Fonseca Bonilla, N. & Ponti, G. 2009, A&A, 495, 421
Bianchi, S., Chiaberge, M., Evans, D. A., Guainazzi, M., Baldi, R. D., Matt, G., & Piconcelli, E. 2010, MNRAS, 418
Crawford, F., Hessels, J. W. T., & Kaspi, V. M. 2007, ApJ, 662, 1183
Chiaberge, M., Capetti, A., & Macchetto, F. D. 2005, ApJ, 625, 716
Dai, H.-F., & Wang, T.-G. 2008, Chinese Journal of Astronomy and Astrophysics, 8, 245
Donato, D., Sambruna, R. M., & Gliozzi, M. 2004, ApJ, 617, 915
Dudik, R. P., Satyapal, S., Gliozzi, M., & Sambruna, R. M. 2005, ApJ, 620, 113
Dunn, R. J. H., Allen, S. W., Taylor, G. B., Shurkin, K. F., Gentile, G., Fabian, A. C.& Reynolds, C. S. 2010 MNRAS, 404, 780
Elvis, M. 2000, ApJ, 545, 63
Emsellem, E., & Ferruit, P.W., 2000, A&A, 357, 111
Eracleous, M., Shields, J. C., Chartas, G., & Moran, E. C. 2002, ApJ, 565, 108
Eracleous, M., Lewis, K. T., & Flohic, H. M. L. G. 2009, New Astronomy Review, 53, 133
Eracleous, M., Hwang, J. A., & Flohic, H. M. L. G. 2010, ApJ, 711, 796
Eracleous, M., Hwang, J. A., & Flohic, H. M. L. G. 2010, ApJS, 187, 135
Filho, M. E., Barthel, P. D., & Ho, L. C. 2002, A&A, 385, 425
González Delgado, R. M., Cid Fernandes, R., Pérez, E. et al. 2004, ApJ, 605, 127
González Delgado, R. M., Pérez, E., Cid Fernandes, R., & Schmitt, H. 2008, AJ, 135, 747
González-Martín et al. (2010, in preparation)
González-Martín, O., Masegosa, J., Márquez, I., & Guainazzi, M. 2009b, ApJ, 704, 1570
González-Martín, O., Masegosa, J., Márquez, I., Guainazzi, M., & Jiménez-Bailón, E. 2009a, A&A, 506, 1107
González-Martín, O., Masegosa, J., Márquez, I., Guerrero, M. A., & Dultzin-Hacyan, D. 2006, A&A, 460, 45
Goudfrooij, P.; de Jong, T.; Norgaard-Nielsen, H. U.; Hansen, L.; Jorgensen, H. E. 1990, A&A, 228, L9
Greene, J. E.; Hood, Carol E.; Barth, Aaron J.; Bennert, Vardha N.; Bentz, Misty C.; Filippenko, Alexei V.; Gates, Elinor; Malkan, Matthew A.; Treu, Tommaso; Walsh, Jonelle L.; Woo, Jong-Hak 2010, arXiv:1009.0532.
Heckman, T. M. 1980, A&A, 87, 152
Ho, L. C., Filippenko, A. V., & Sargent, W. L. W. 1997, ApJ, 487, 568
Ho, L. C. 1999, ApJ, 516, 672
Ho, Luis C.; Feigelson, Eric D.; Townsley, Leisa K.; Sambruna, Rita M.; Garmire, Gordon P.; Brandt, W. N.; Filippenko, Alexei V.; Griffiths, Richard E.; Ptak, Andrew F.; Sargent, Wallace L. W.Ho, L. C., et al. 2001, ApJ, 549, L51
Ho, L. C. 2002, ApJ, 564, 120
Ho, L. C. 2008, ARA&A, 564, 120
Laine, S., van der Marel, R. P., Rossa, J., Hibbard, J. E., Mihos, J. C., Böker, T., & Zabludoff, A. I. 2003, AJ, 126, 2717
Maiolino, R.; Comastri, A.; Gilli, R.; Nagar, N. M.; Bianchi, S.; Bker, T.; Colbert, E.; Krabbe, A.; Marconi, A.; Matt, G.; Salvati, M. 2003, MNRAS, 344, L59
Malizia, A.; Stephen, J. B.; Bassani, L.; Bird, A. J.; Panessa, F.; & Ubertini, P. 2009, MNRAS, 399, 944
Maoz, D., Filippenko, A. V., Ho, L. C., Rix, H.-W., Bahcall, J. N., Schneider, D. P., & Macchetto, F. D. 1995, ApJ, 440, 91
Maoz, D., Nagar, N. M., Falcke, H., & Wilson, A. S. 2005, ApJ, 625, 699
Maoz, D. 2007, MNRAS, 377, 1696
Márquez, I., Masegosa, J., Moles, M., Varela, J., Bettoni, D., & Galletta, G. 2003, Ap&SS, 284, 711
Nagar, N. M., Falcke, H., Wilson, A. S., & Ho, L. C. 2000, ApJ, 542, 186
Nagar, N. M., Falcke, H., Wilson, A. S., & Ulvestad, J. S. 2002, A&A, 392, 53
Nagar, N. M., Falcke, H., & Wilson, A. S. 2005, A&A, 435, 521
Panessa, F., Bassani, L., Cappi, M., Dadina, M., Barcons, X., Carrera, F. J., Ho, L. C., & Iwasawa, K. 2006, A&A, 455, 173
Panessa, F.; Bassani, L.; de Rosa, A.; Bird, A. J.; Dean, A. J.; Fiocchi, M.; Malizia, A.; Molina, M.; Ubertini, P.; Walter, R. 2008 A&A, 483, 151
Peterson, B. M.; Berlind, P.; Bertram, R.; Bischoff, K.; Bochkarev, N. G. et al. 2002, ApJ, 581, 197
Pian, E., Romano, P., Maoz, D., Cucchiara, A., Pagani, C., & Parola, V. L. 2010, MNRAS, 401, 677
Pogge, R. W., Maoz, D., Ho, L. C., & Eracleous, M. 2000, ApJ, 532, 323
Sarzi, M.; Falcón-Barroso, J.; Davies, R.L.; Bacon, R.; Bureau, M.et al. 2006, MNRAS, 366, 1151
Schmitt, H. R., Donley,J. L., Antonucci, R. R. J., Hutchings, J. B., Kinney, A. L., & Pringle, J. E. 2003, ApJ, 597, 768
Shapiro, K. L., Cappellari, M., de Zeeuw, T., McDermid, R. M., Gebhardt, K., van den Bosch, R. C. E., & Statler, T. S. 2006, MNRAS, 370, 559
Shields, J. C.; Rix, H.-W.; Sarzi, M.; Barth, A.J.; Filippenko, A.V. et al. 2007, ApJ, 654, 125
Simões Lopes, R. D., Storchi-Bergmann, T., de Fátima Saraiva, M., & Martini, P. 2007, ApJ, 655, 718
Starling, R. L. C.,Page, M. J., Branduardi-Raymont, G., Breeveld, A. A., Soria, R., & Wu, K. 2005, MNRAS, 356, 727
Urry, C. M., Padovani, P. 1995 PASP, 107, 803
van Dokkum, P.G. 2001 PASP, 113, 1420
Veilleux, Sylvain; Cecil, Gerald; Bland-Hawthorn, Joss 2005 ARA&A, 43, 769
Verdoes Kleijn, G. A., Baum, S. A., de Zeeuw, P. T., & O'Dea, C. P. 1999, AJ, 118, 2592
Walsh, J. L., Barth, A. J., Ho, L. C., Filippenko, A. V., Rix, H.-W., Shields, J. C., Sarzi, M., & Sargent, W. L. W. 2008, AJ, 136, 1677
Worrall, D. M., Birkinshaw, M., Laing, R. A., Cotton, W. D., & Bridle, A. H. 2007, MNRAS, 380, 2
Worrall, D. M., Birkinshaw, M., & Hardcastle, M. J. 2003, MNRAS, 343, L73
Wu, Q. & Cao, X. 2005 ApJ, 621, 130

Appendix A: Comments on individual objects

IC 1459. At HST resolution Lauer et al. (2005) classified this galaxy as an starting dusty nuclear ring and Verdoes Kleijn et al. (2000), based in Hα+[NII] WFPC2 images, identify an ionized gas disk with PA 37^o and inclination 60^o following what is found by Goudfrooij et al. (1990) at larger scales (100 arcsec). Here we report a residual Hα emission with a central source and a rather biconical distribution extended ~ 500 pcs at PA 37^o (Fig. 2). At soft X-ray energies (0.3-2 keV), it extends along the same direction than that in Hα HST data (Fig. 6).

NGC 315. A compact unresolved source of ionized gas on top of a dusty disk, together with an extension of the disk of 200 pc at PA 49^o is detected (see Fig. 2; see also Verdoes-Keijn et al. 1999). The high spatial resolution provided by Chandra imaging allowed the detection of the X-ray jets (Donato et al., 2004; Worrall et al., 2003, 2007; Gonzalez-Martin et al. 2009). Soft X-rays are extended along the axes of the jet and the host galaxy (Fig. 6).

NGC 2639. At HST resolution, its Hα shows an elongated asymetric extended structure at PA -29^o, but not nuclear compact source is identifiable. It also shows extended filaments

being more prominent towards the NW. The SE region is maybe obscured by dust. The SD images and the broad band data show a rather dusty morphology (see Fig. 2 and Simões Lopez et al. 2007).

NGC 2681. The Hα emission image show a central source with extended emission along the central spiral structure with major axis at PA 40^o and a radial extension of 4 arcsecs ($\sim$ 440 pcs). Spiral dust lanes are clearly detected in the SD image (Fig. 2). Broad agreement is found in the elongation of soft X-ray and Hα emissions (Fig. 6).

NGC 2787. On the HST SD images, a near-nuclear dust-lane is clearly resolved into a spectacular set of concentric, elliptical dust rings, covering a radial range of 510″(see also Shields et al. 2007, Simões-Lopes et al. 2008, Gonzalez Delgado et al. 2008). In Hα, a nuclear component has been detected, in good agreement with Dai & Wang (2009). An elongation at PA 49^o can also be identified, which is perpendicular to the major axis of the galaxy (Fig. 2). Soft X-rays roughly follow the Hα emission (Fig. 6).

NGC 2841. At HST resolutions it shows a rather face-on ring-like structure and a clearly well identified unresolved nuclear source. A small NLR can be identified at PA of 90^o. Dust morphology becomes apparent from the SD image (Fig. 2). Soft X-rays extend along two main axes, one following the hard X-ray emission (PA about 10) and the other one close to that of the Hα emission (Fig. 6).

NGC 3226. This galaxy shows a bright nucleus with some evidences of dusty environment clearly seen in the SD image (see also Gonzalez Delgado et al. 2008) . In H_α it shows an extended morphology quite similar to that observed in continuum (Fig. 2). At X-ray frequencies it shows a compact structure both at soft and hard energies. The Hα however seems to suggest an outflow-like morphology coming out from that compact nucleus (Fig. 6).

NGC 3245. The H_α image shows a kidney-like structure slightly brighter to the North, with a nuclear unresolved source (see also (Gonzalez Delgado et al. 2008, Walsh et al. 2008). Kinematical data from Walsh et al. (2008) support our outflow classification. The western dust structure is clearly appreciated in the SD image. (Fig. 2). One of the two axes shown by the soft X-ray contours follows the Hα emission (Fig. 6).

NGC 3379. An extended structure emerging from the nucleus can be apreciated althought the S/N ratio on the Hα image is low. A tiny dust-lane crosses the nuclear regions at PA -50 in SD (Fig. 2). At HST resolution Lauer et al. (2005), based in the F555W filter, classified this galaxy without a clear nuclei but with a dusty nuclear ring morphology. Shapiro et al. (2006) reported a well defined disk of emission at Hα with PA 118. The morphology of the soft X-ray contours is quite complex, but a rough agreement with the extended Hα emission is found (Fig. 6).

NGC 3607. The Hα image shows a clearly nuclear unresolved source and diffuse emission following what it appears to be an inclined disk. The strong dust lanes visible in the SD images obscure the Hα emission (Fig. 2). Lauer et al. (2008) suggested that it contains a dusty outer disk dynamically old which appears to transition rapidly but smoothly at the center to a second gas disk that is perpendicular to the first and is seen nearly edge-on. This inclined disk seems to be settling onto a nuclear ring. Excepting the outermost contours, the soft X-ray emission elongates along the Hα emission (Fig. 6).

NGC 3623. Hα emission has been detected, extending $\sim$ 130 pc at PA -10^o. Inside the more extended structure an inner disk is appreciated extending 30 parsecs along PA 53^o. Large scale dust-lanes clarly appear in the SD image (Fig. 2).

NGC 3627. The H_α data (Fig. 2) do not show a well defined nuclear source, most probably due to the dust lane crossing the nuclear region in the direction NS and obscuring the SE-NW elongated extended emission (see the SD image). Gonzalez-Delgado et al. 2008 reported from HST data that chaotic dust lanes and several compact sources are identified at the center.

NGC 3998. The Hα image (Fig. 2) shows a 100 pc extended structure surrounding a compact nucleus. The major axis of this extension is oriented along a PA=0 (see also Pogge et al. 2000). The SD image shows little indication of dust in the nuclear region, in good agreement with Gonzalez Delgado et al. (2008). Soft X-rays are elongated along the same direction as the Hα emission (Fig. 6).

NGC 4036. The HST Hα image (Fig. 2) shows, on top of a well identified nuclei, the existence of a complicated filamentary and clumpy structure, with an extension of 390 pcs at PA 63^o, already reported by Pogge et al. (2000) and Dai and Wang (2009) (see also the SD image). Walsh et al. (2009) have shown the presence of a gas velocity gradient of $\sim$ 300 km s^{-1} across the inner 0.2”, compatible with the outflow-like structure apparent in the ionised gas. The soft X-ray emission appears to follow the Hα emission (Fig. 6).

NGC 4111. A rather knotty morphology surrounding a clear nuclear source is observed, embebed in a diffuse halo. This morphology is interpreted as a core-halo structure detected at HST resolution both with medium size filters (Simões Lopes et al. 2007) and narrow band Hα data (Dai and Wang, 2009). A crossing dust structure is seeing perpendicular to the disk main plane (see SD image). Soft X-ray contours are elongated along the same PA as the Hα emission (Fig. 6).

NGC 4278. A clear core-halo morphology is shown by its Hα emission on the top of a very faint continuum (Fig. 2). This emission seems to follow what it is observed in the soft X-ray emission (Fig. 6).

NGC 4314. The Hα image (Fig. 2) shows both an unresolved nucleus and a number of HII regions tracing the star formation ring. The same features are well traced by the SD image, where the spiral dust lanes associated with the ring are conspicuous (see also Gonzalez Delgado et al. 2008). At soft energies, its emission follow the star forming regions observed in Hα (Fig. 6).

NGC 4374. Hα image (Fig. 2) shows an inclined gas disk surrounding the nucleus. This emission gas structure takes the form of filaments that extend roughly east-west and north-south (see also (Pogge et al. 2000). The dust structure clearly appears in the SD image, where the nucleus is seen in the center of the dust-lane to the South. The soft X-ray contours are roughly aligned with the ionised gas (Fig. 6).

NGC 4438. Gonzalez Delgado et al(2008) defined it as galaxy with very perturbed central morphology and strong dust lanes cross the center along PA 0 obscuring the eastern side of the galaxy (see the SD image). The Hα image (Fig. 2) shows a ring-like structure where a clear knot is seen in the south-east region coincident with the continuum nucleus. The other side would remain invisible due to obscuration by dust. Two plumes can be apreciated to the north and south west extending about 150 pcs in both directions. This is one of the clearest examples to be a candidate of nuclear outflow, buble structures, as defined in Veilleux and Brandt (2007). Soft X-rays are aligned with the Hα emission (Fig. 6).

NGC 4486. The Hα image (Fig. 2) shows a compact source with filaments which resemble an outflow from the nucleus (see also Pogge et al. 2000; Dai and Wang 2009). As already noticed by Pogge et al. (2000), the conpiscous jet clearly visible in the continuum images (see SD) dissapears in the Hα continuum substrated map. Soft X-rays are missaligned with respect to Hα emission, the former following the jet axis (Fig. 6).

NGC 4552. At HST resolution the Hα data show a compact unresolved nuclear source located at the center of a symmetric extended emission in a disk-like structure. No trace of dust-lanes is seen in the SD image (Fig. 2). Soft X-rays roughly follow the Hα emission (Fig. 6).

NGC 4579. The Hα emision (Fig. 2) traces a bright, nuclear point source surrounded by complex clumpy and filamentary emission (see also Pogge et al. 2000). The higher ionization gas traced by [OIII] (Fig. 2) is composed of a compact source and a filamentary, jet-like structure towards the NE. Walsh et al. (2008) have shown that the gas is not in regular rotation, displaying two kinematical components with a velocity separation of 450 km s^{-1}, being consistent with an outflow from the nucleus. The dust-lanes seen in the SD image conform a mainly chaotic structure together with a much stronger, offset, linear feature that goes at PA$\approx$45 in the West side. Soft X-ray contorus follow the Hα emission at large scales. There is a hint of an extension of hard X-rays along the PA of the [OIII] jet-like feature (Fig. 6).

NGC 4594. The Hα image (Fig. 2) shows a compact nuclear source together with fainter emission extending along the E-W direction in a bar-like morphology, with two spiral arms emerging from it, with a total extension of 300 pc. The kinematical data by Walsh et al. (2008) show organized motion consistent with rotation but with significant irregularities in the nucleus. A strong velocity gradient and decoupled kinematics between gas and stars were found by Emsellem & Ferruit (2000). An overall extension of soft X-rays is seen along the same axis as the extended ionised gas (Fig. 6).

NGC 4636. The Hα data (Fig. 2) show a central compact source and a very faint ring like structure more clearly visible in the southern region of the galaxy (see also Simões Lopes et al. 2007 and Dai and Wang 2009). Towards the north, a more prominent Hα emission is seeing with a clear outflow-like morphology. This morphology seems to follow the soft X-ray data (Fig. 6).

NGC 4676A and B. The Mice. The Hα images (Fig. 2) show in both galaxies a very clumpy and irregular structure. In galaxy B a more conspicuous knotty structure is visible (one of the knots coincides with the nucleus). In galaxy A however a more diffuse emission is seen. Central dust-lanes are much stronger in galaxy B, as can be appreciated in the SD images (see also Laine et al. 2003). The soft X-ray contours are unrelated to the extended Hα emission in both galaxes (Fig. 6).

NGC 4696. Hα imaging (Fig. 2) shows a clear nuclear source with elongated extended emission along PA 47^o, and larger filamentary structures towards the west maybe resembling outflows out of the nucleus.Crawford et al (2005) report also a filamentary structure shared by the Hα and soft X-ray emission (see also our Fig. 6).

NGC 4736. The Hα image shows a circumnuclear spiral structure of extension 200 pc. Dust lanes in spiral arms are traced in the SD image (Fig. 2). Gonzalez Delgado et al. (2008) suggest the presence of spiral dust lanes down the nucleus and a compact nuclear stellar cluster. Despite the complexity of the soft X-ray emission, a rough agreement is found in the overall shape of both images (Fig. 6).

NGC 5005. Hα data (Fig. 2) show a very asymmetric emission with a wide-angle cone-like structure extending to the SE (see Pogge et al. 2000 and Dai & Wang 2009), perpendicular to the major axis of the galaxy. A strong dust lane crosses the galaxy from East to West, offset from the nucleus (see the SD image and Gonzalez Delgado et al. 2008).

NGC 5055. Its Hα image (Fig. 2) shows a nuclear source and extended emission along PA 110^o. A floculent spiral structure, stronger to the Souht, is visible in the SD image (see also Gonzalez Delgado et al. 2008). Soft X-rays and Hα emission are extended along roughly the same direction (Fig. 6).

NGC 5846. The Hα image (Fig. 2) shows a compact nucleus and diffuse emission resembling a very wide outflow extending up to 2" in the W direction. This strong asymmetry cannot be explained by dust absorption (see the SD image). No correaltion is seen between Hα and soft X-ray emission (Fig. 6).

NGC 5866. The Hα image shows an extremely faint nucleus on top of a very dusty structure along PA -45^o strongly obscuring the nucleus (see also the SD image) what hampers either any classification of the emission (Fig. 2) or any comparison with the soft X-ray emission (Fig. 6).

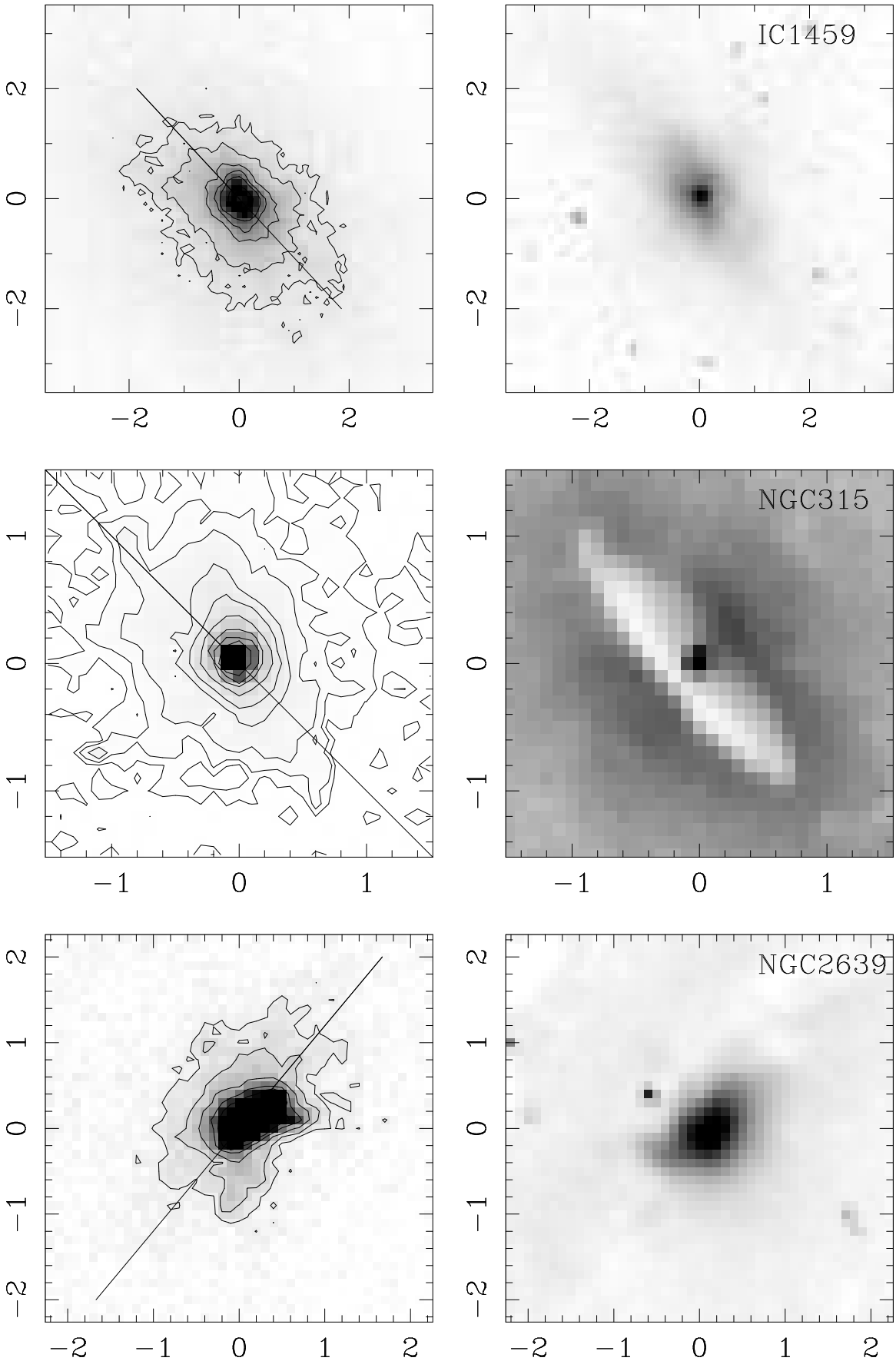

Fig. 2. Images of Hα (left) and SD (right). Top is north and east is left. The units of the plots are arcseconds. For clarity contours above 3σ levels have been plotted in the Hα images. For the outflow candidates the contour for which R^*_{eq} has been estimated is also plotted in black or white thick line. The position angle of the host major axis has been taken from the ned database and it is shown as a solid line.

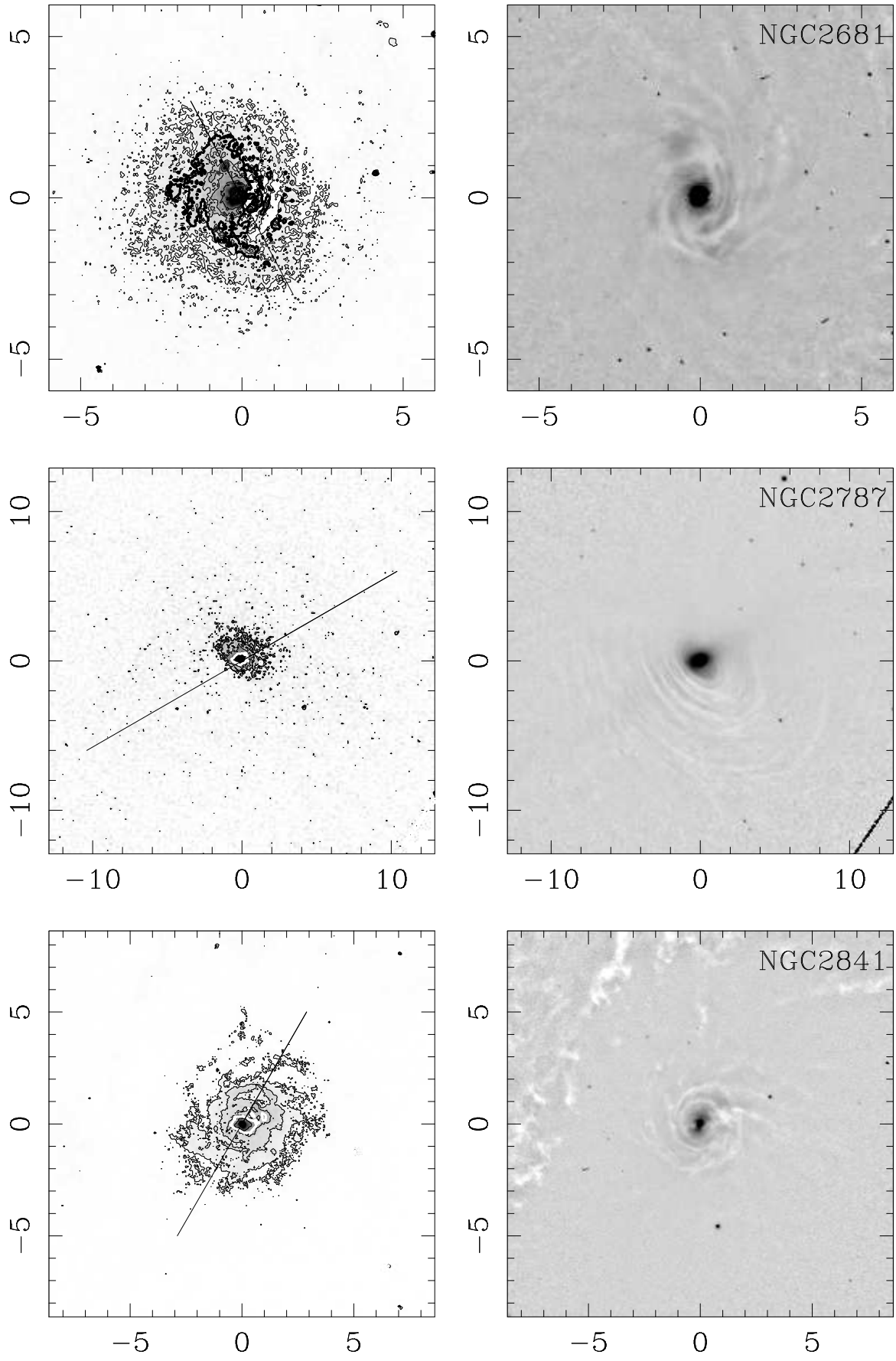

Fig. 2. Continued.

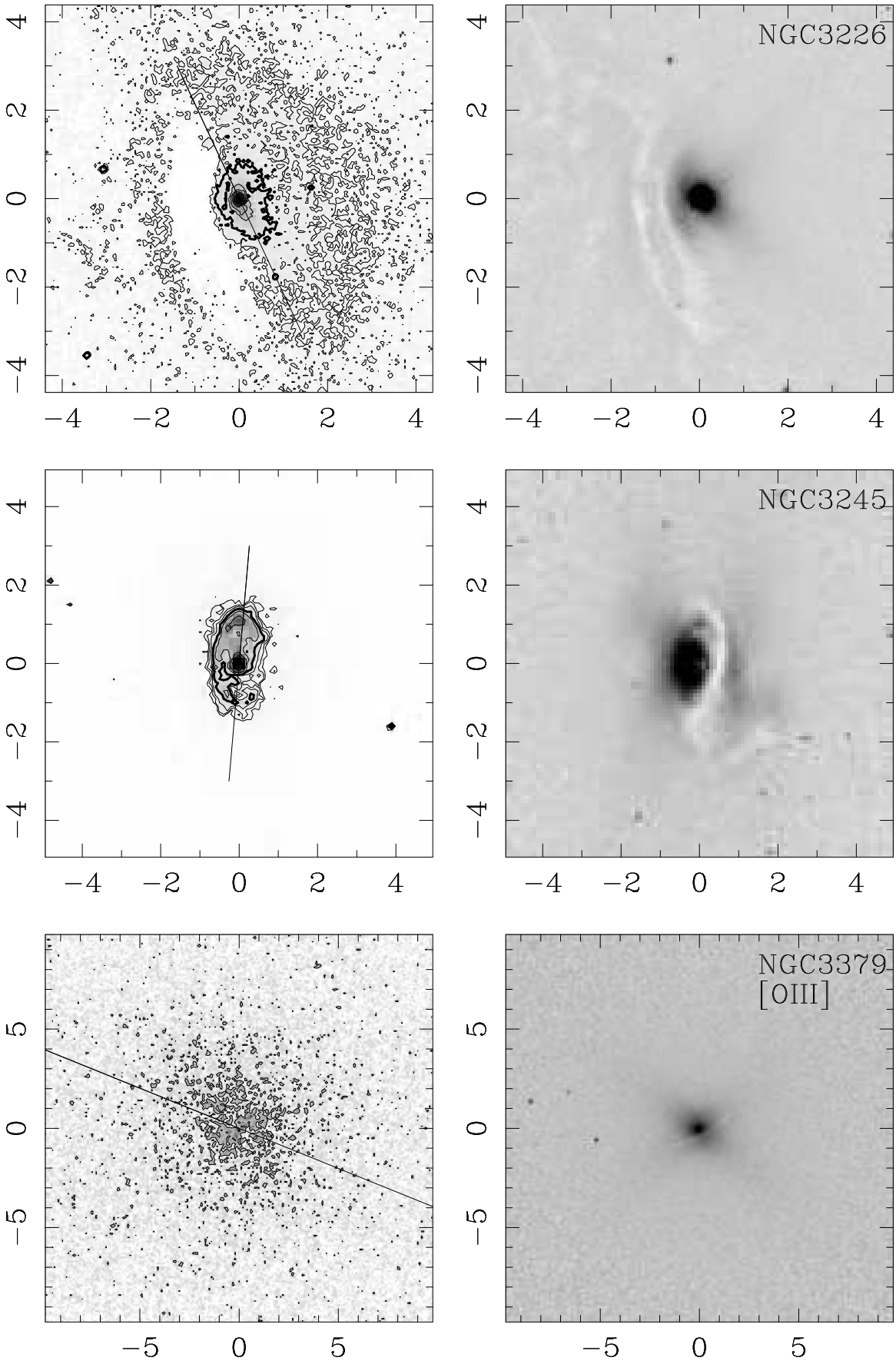

Fig. 2. Continued.

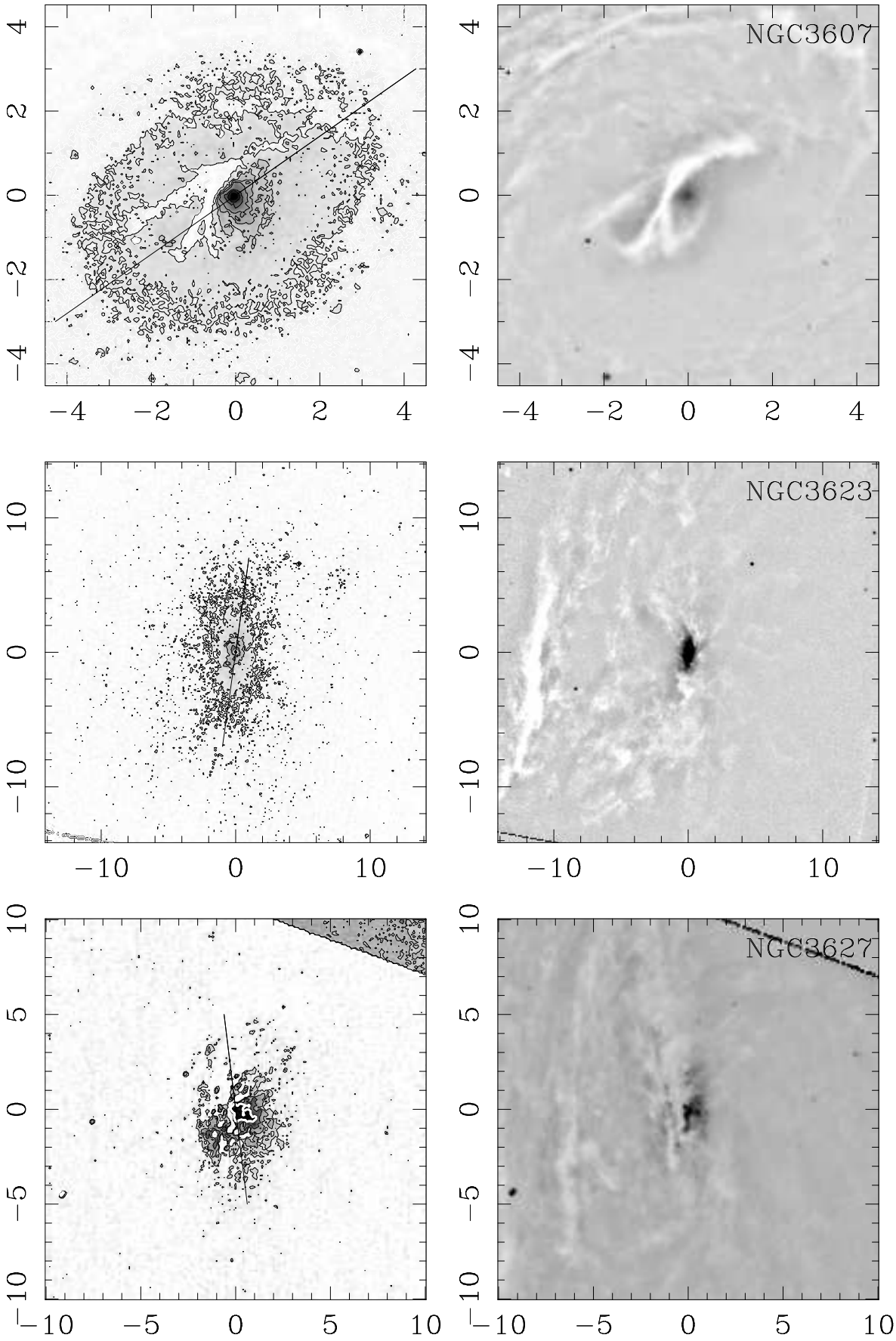

Fig. 2. Continued.

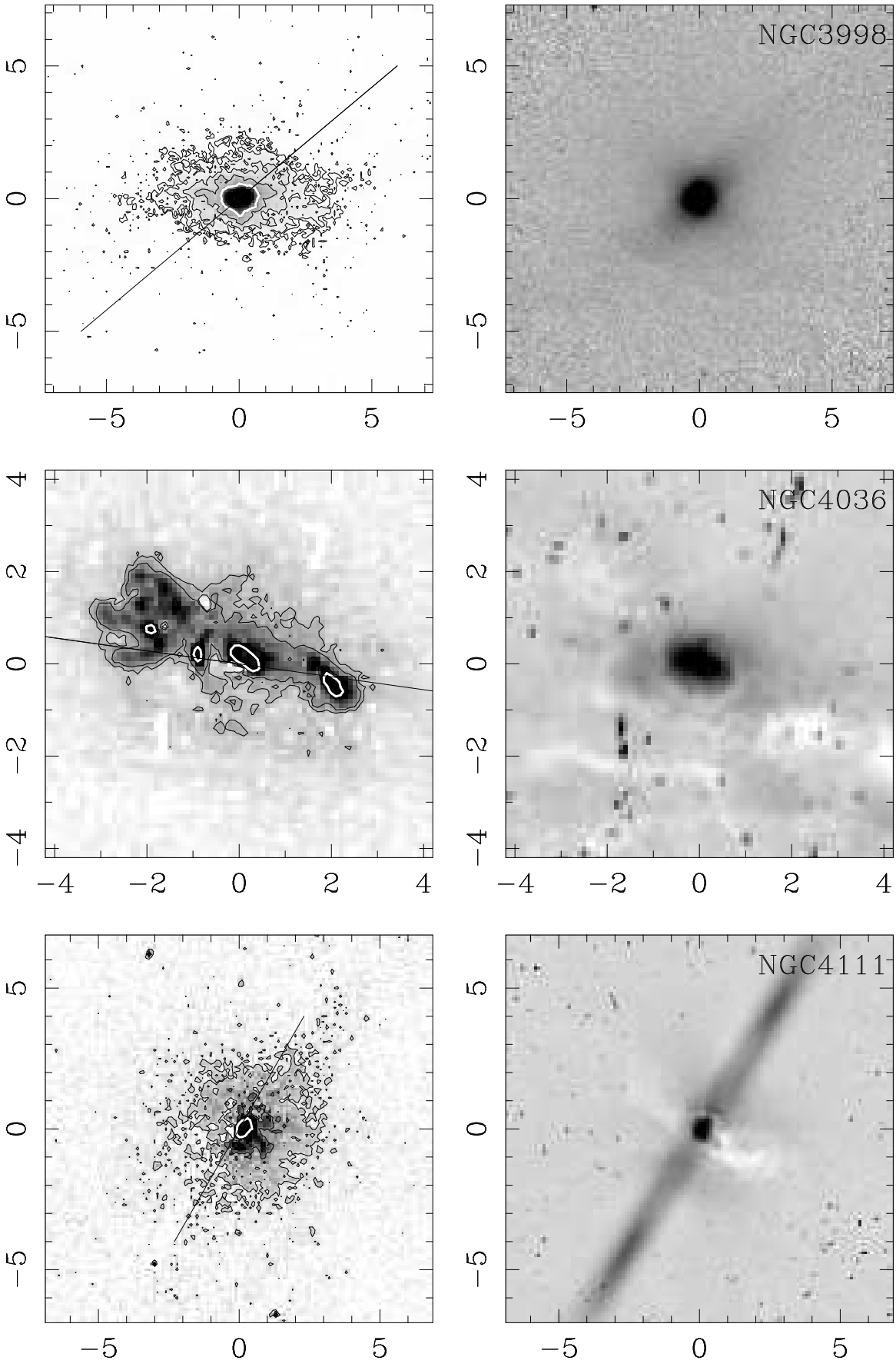

Fig. 2. Continued.

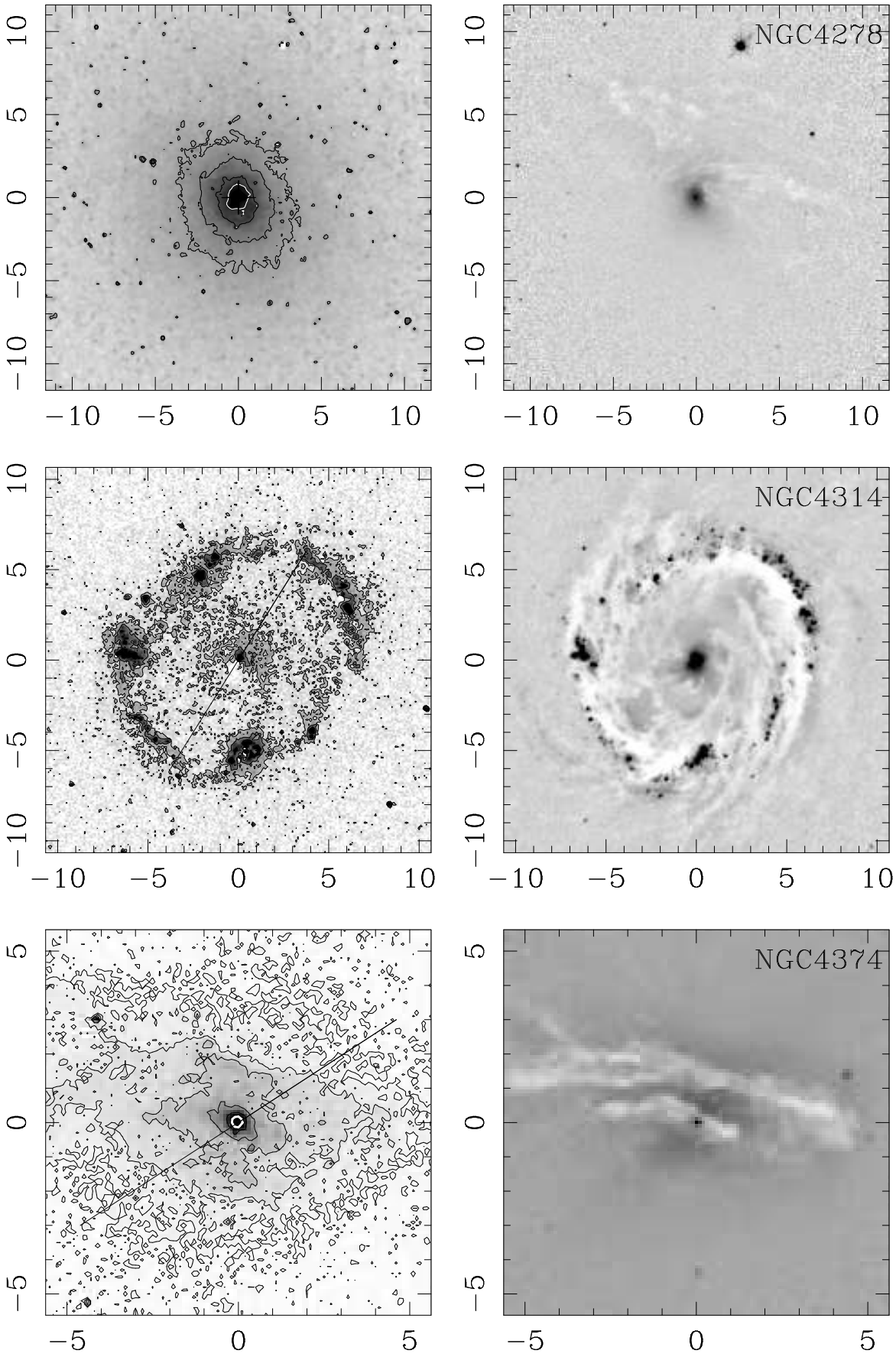

Fig. 2. Continued.

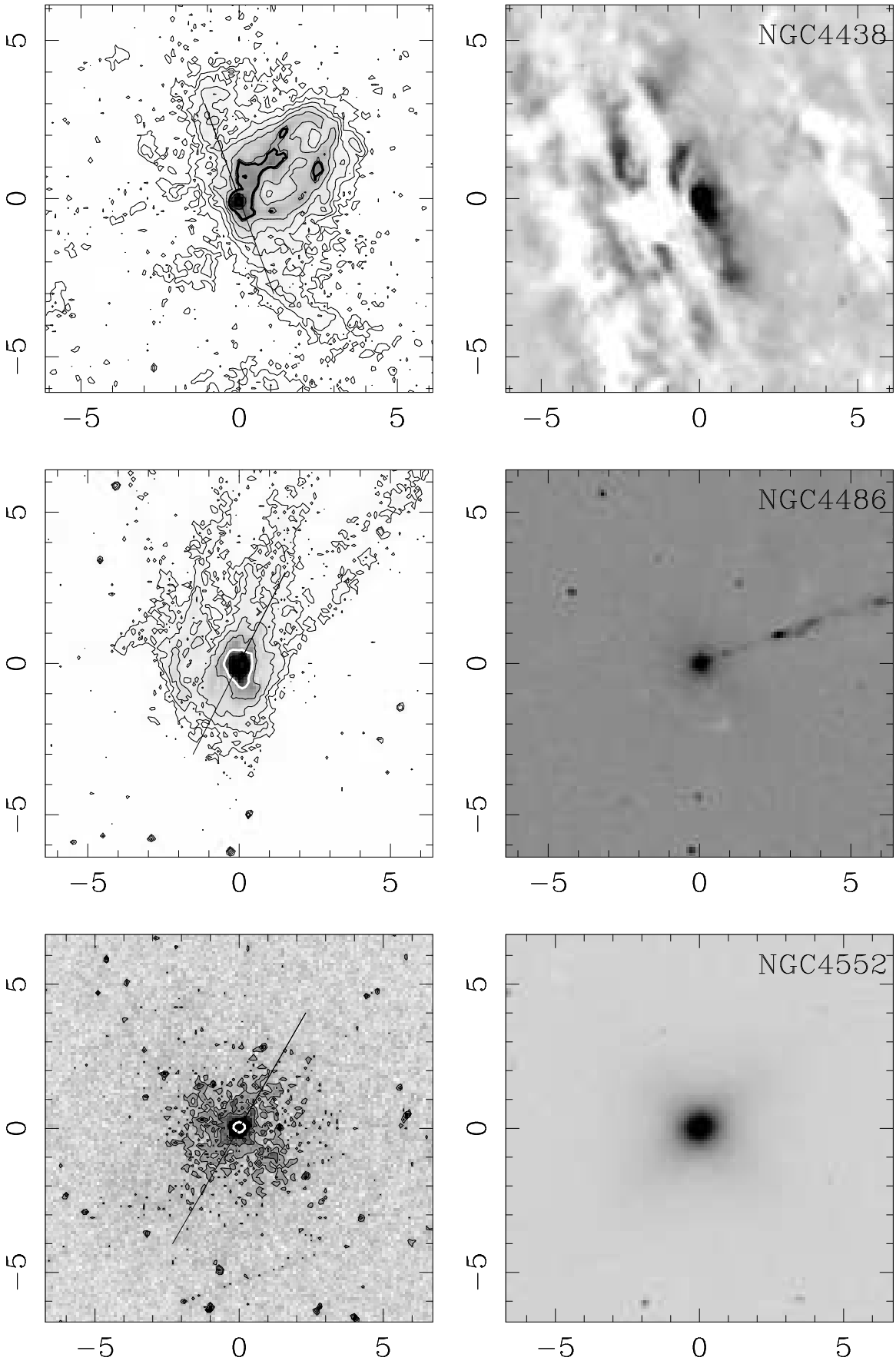

Fig. 2. Continued.

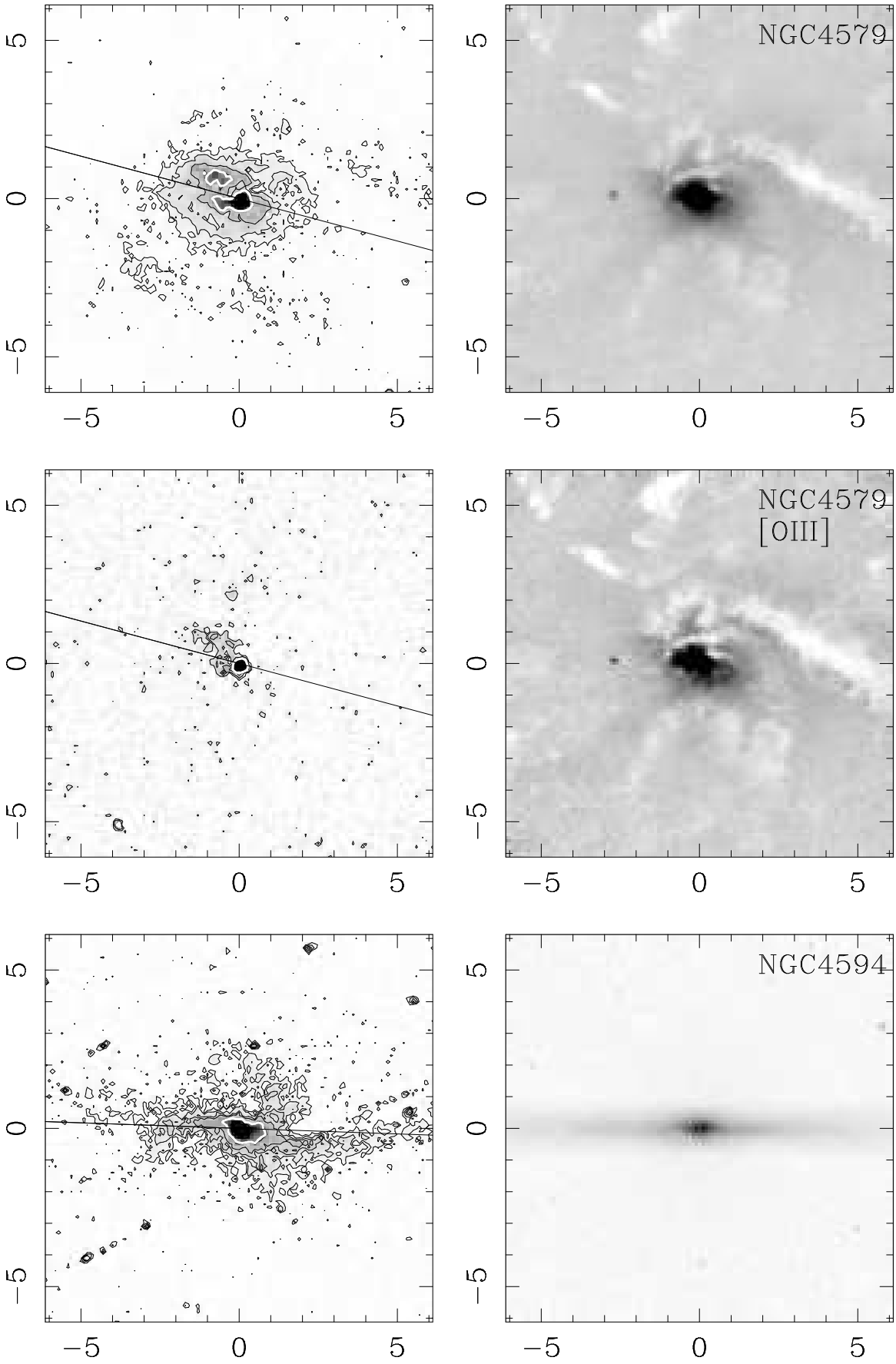

Fig. 2. Continued.

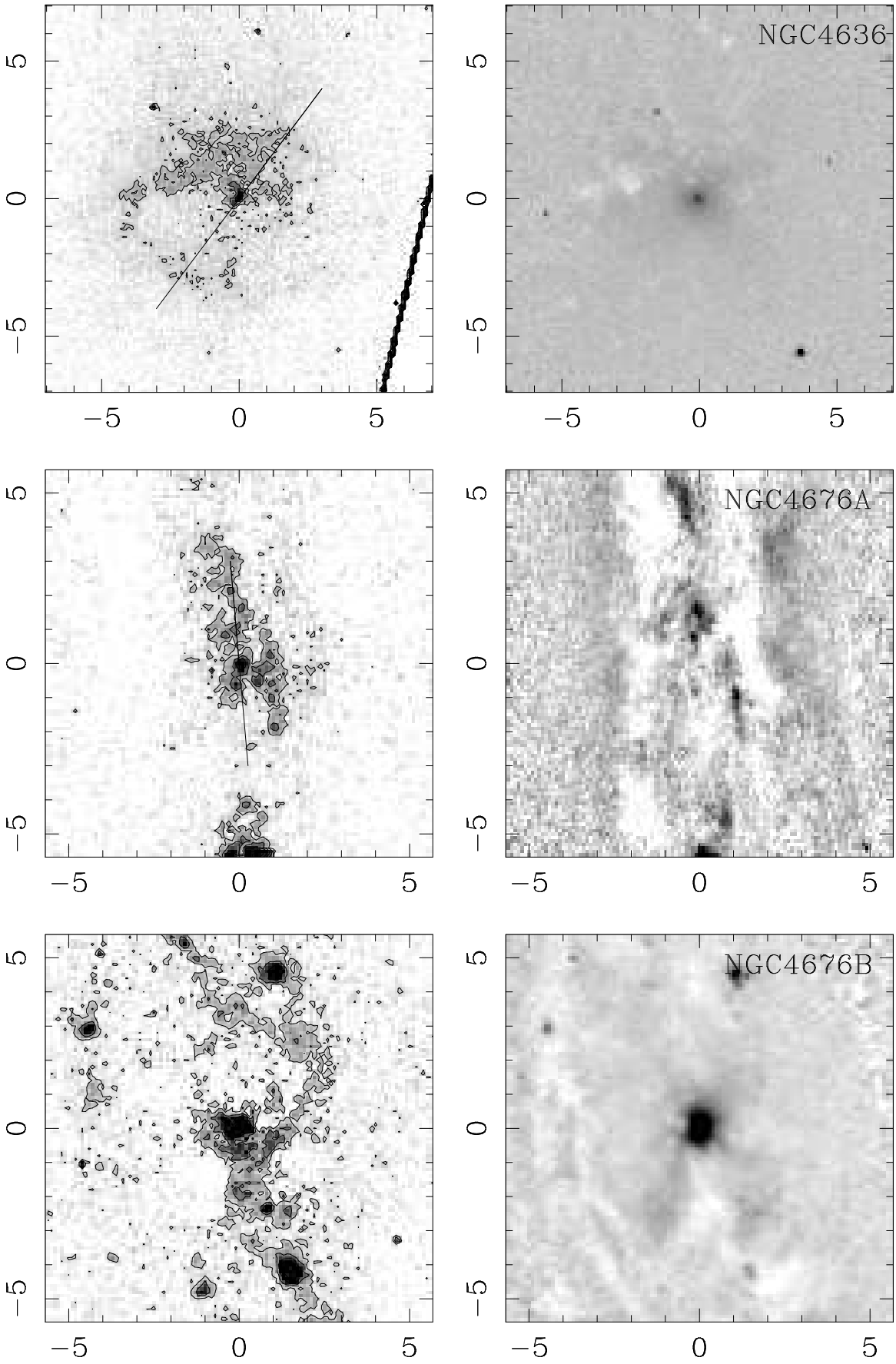

Fig. 2. Continued.

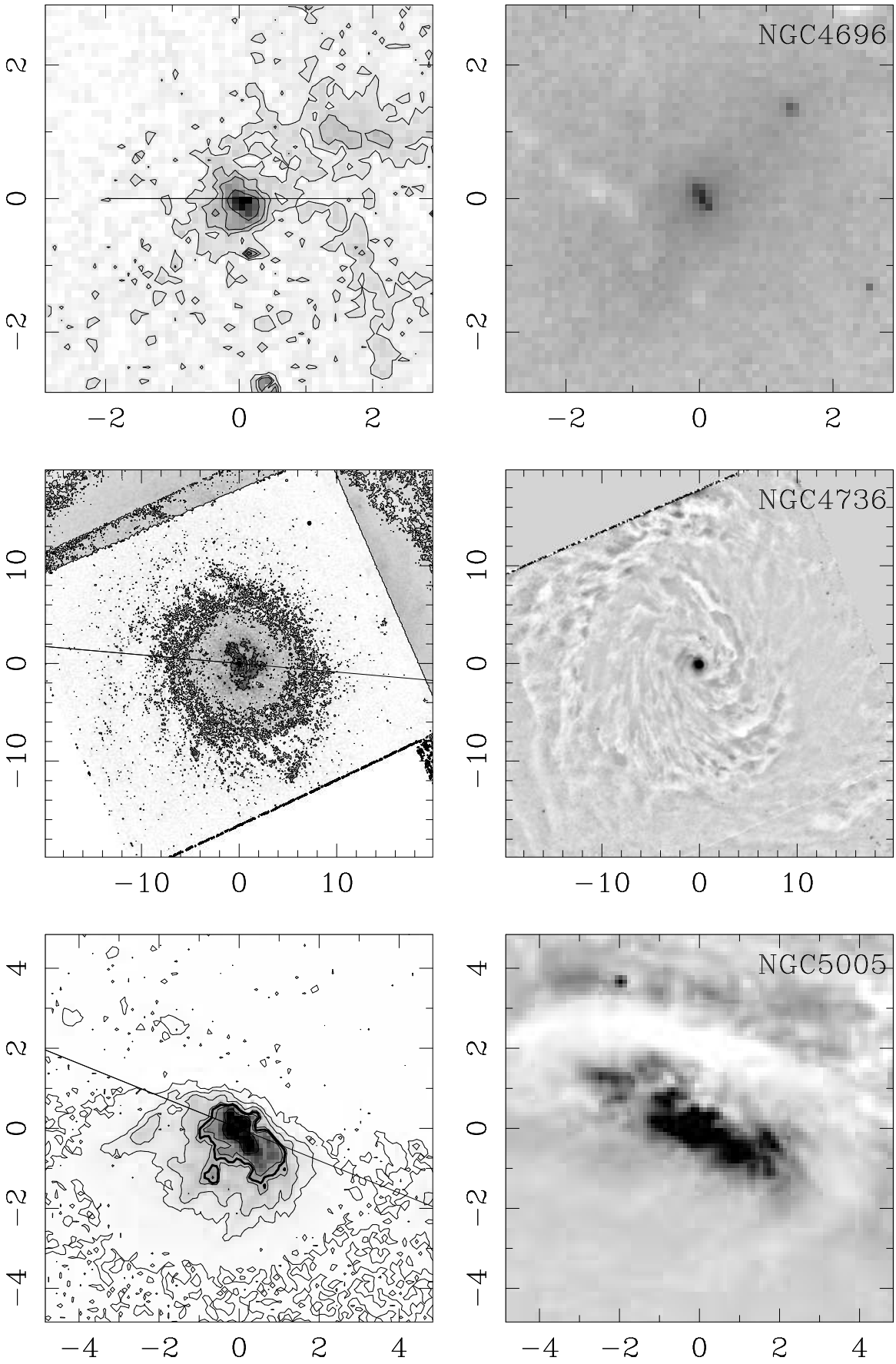

Fig. 2. Continued.

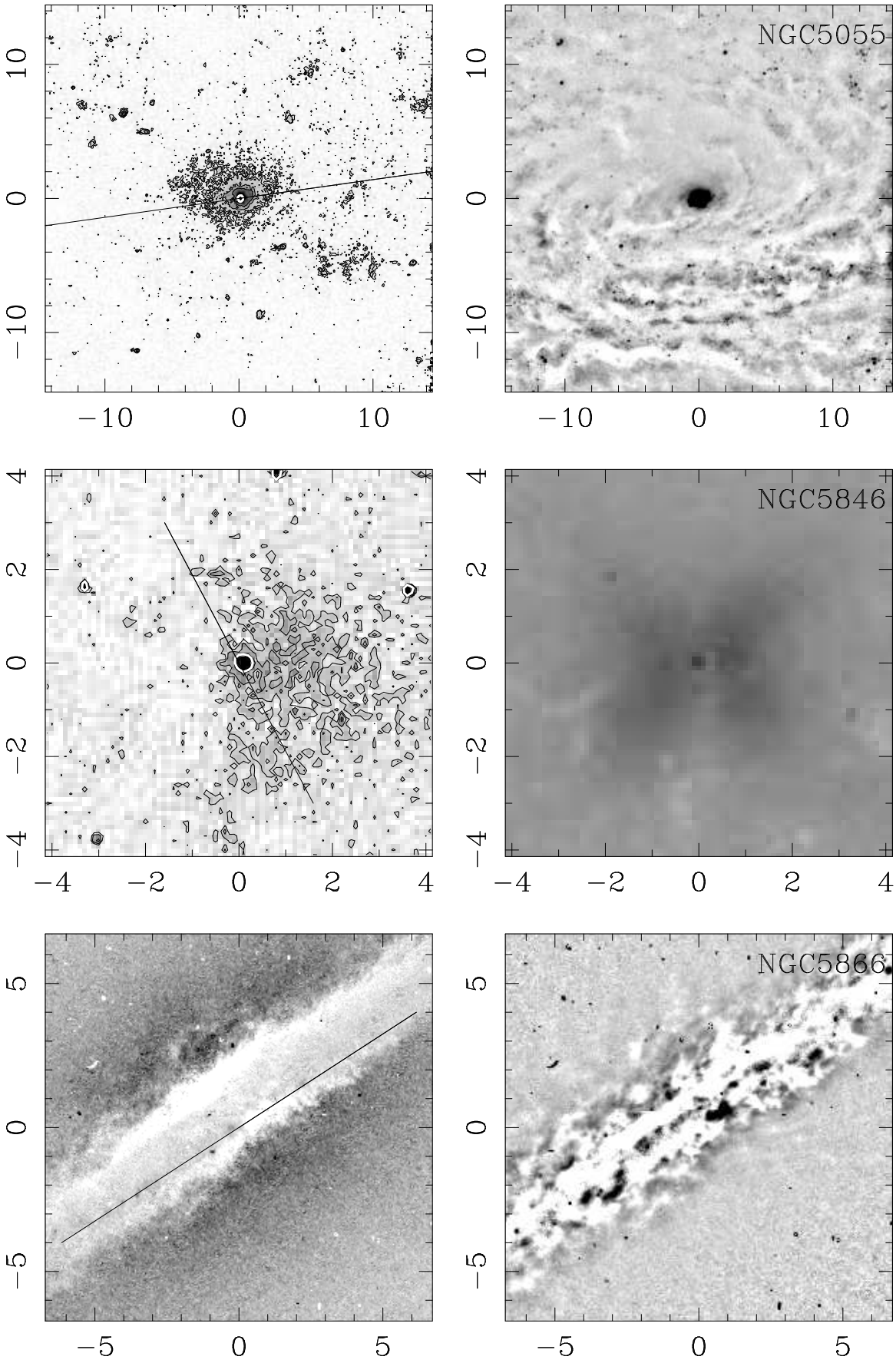

Fig. 2. Continued.

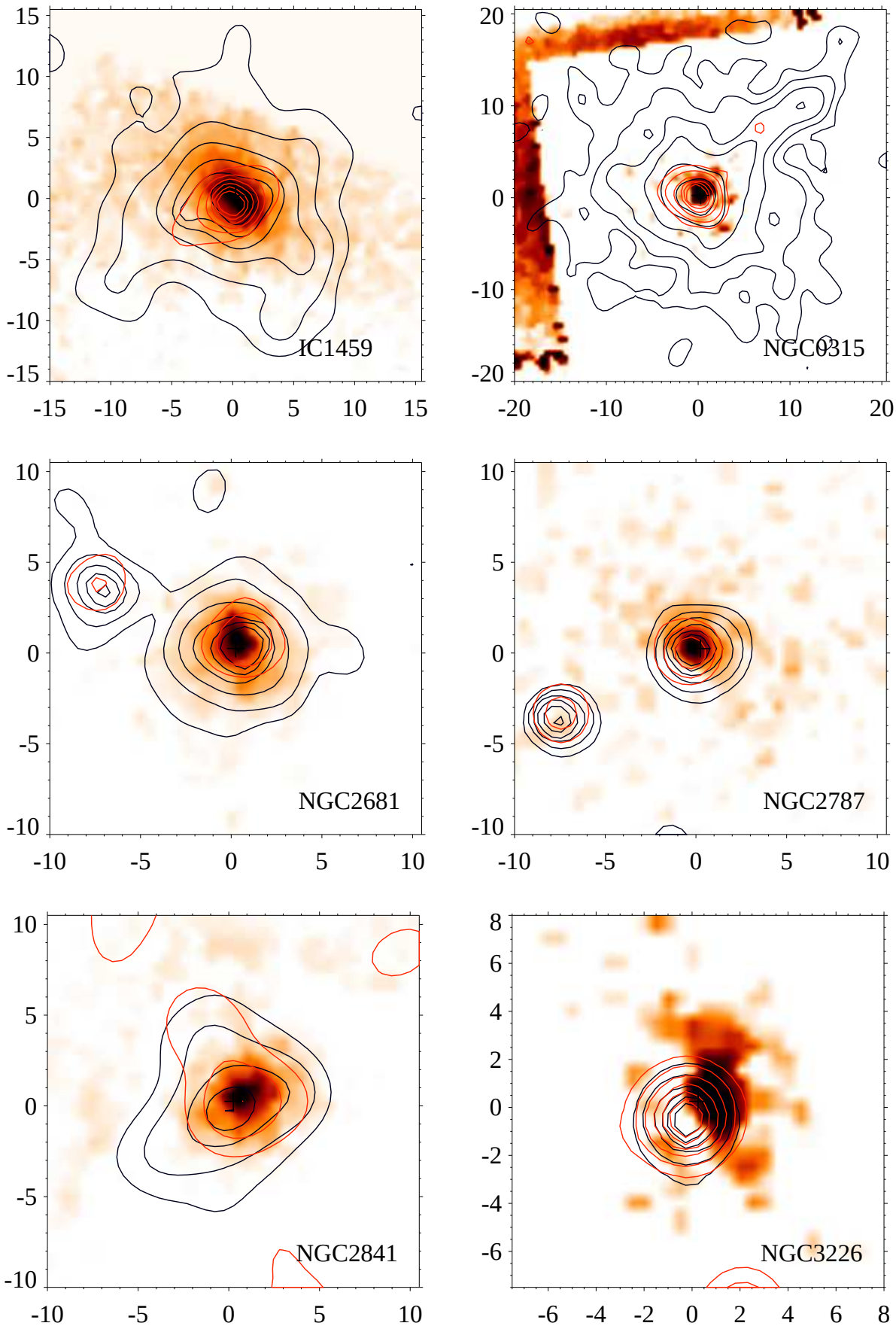

Fig. 6. X-ray contours are overplotted onto the Hα images. Top is north and east is left. The units of the plots are arcseconds. Soft (0.6-0.9 keV) X-rays contours are plotted in black and hard (4.5-8 keV) X-rays in red

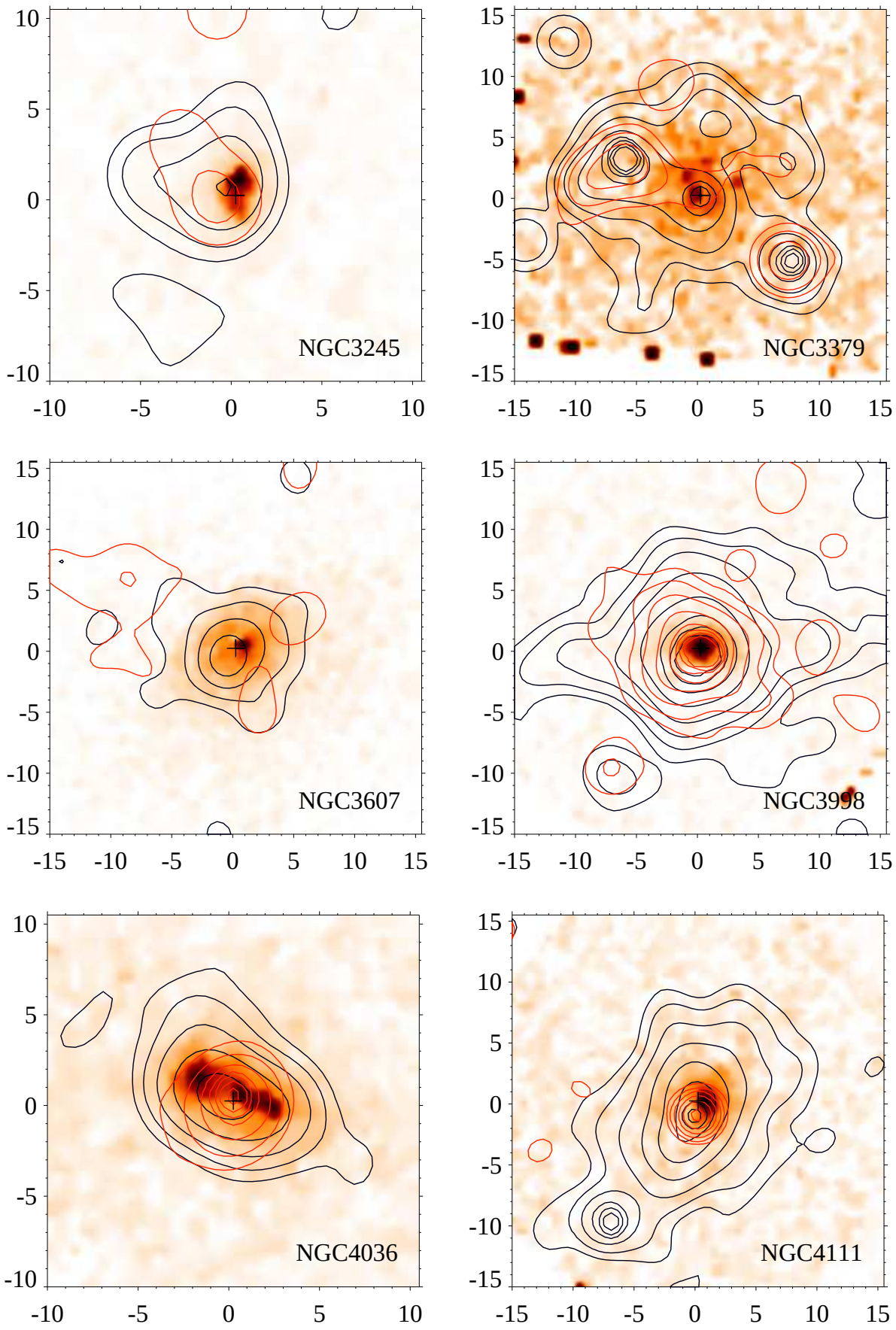

Fig. 6. Continued.

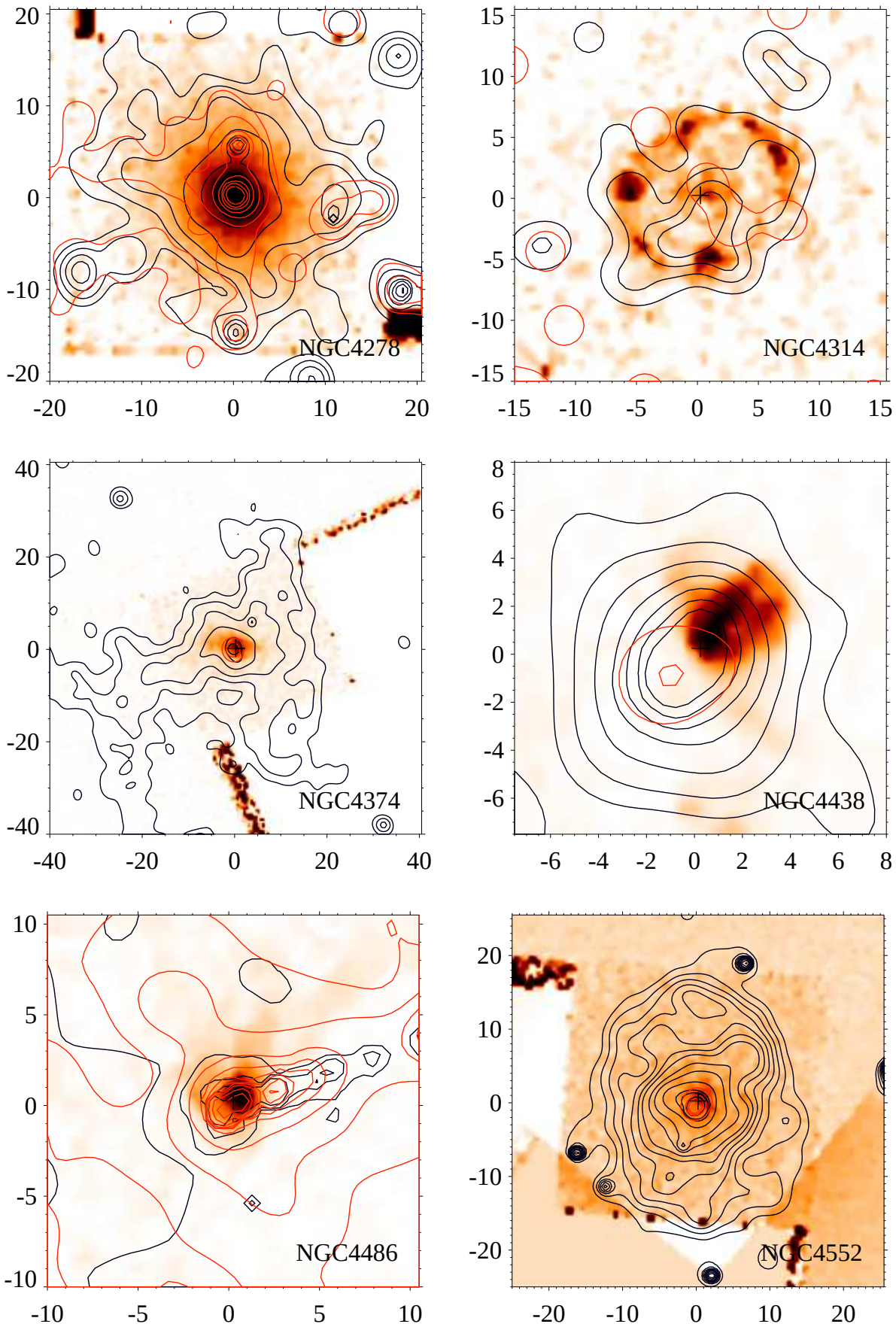

Fig. 6. Continued.

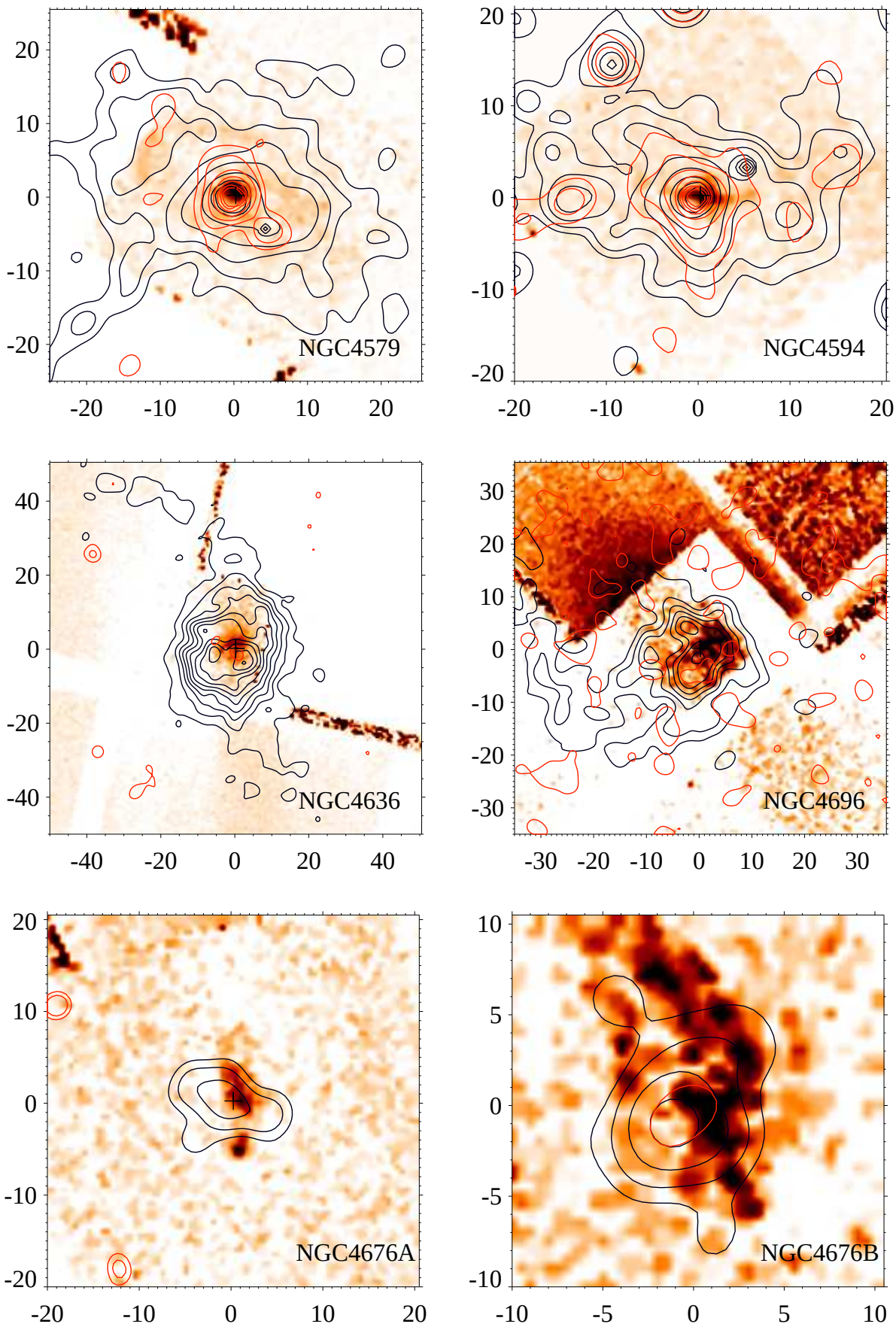

Fig. 6. Continued.

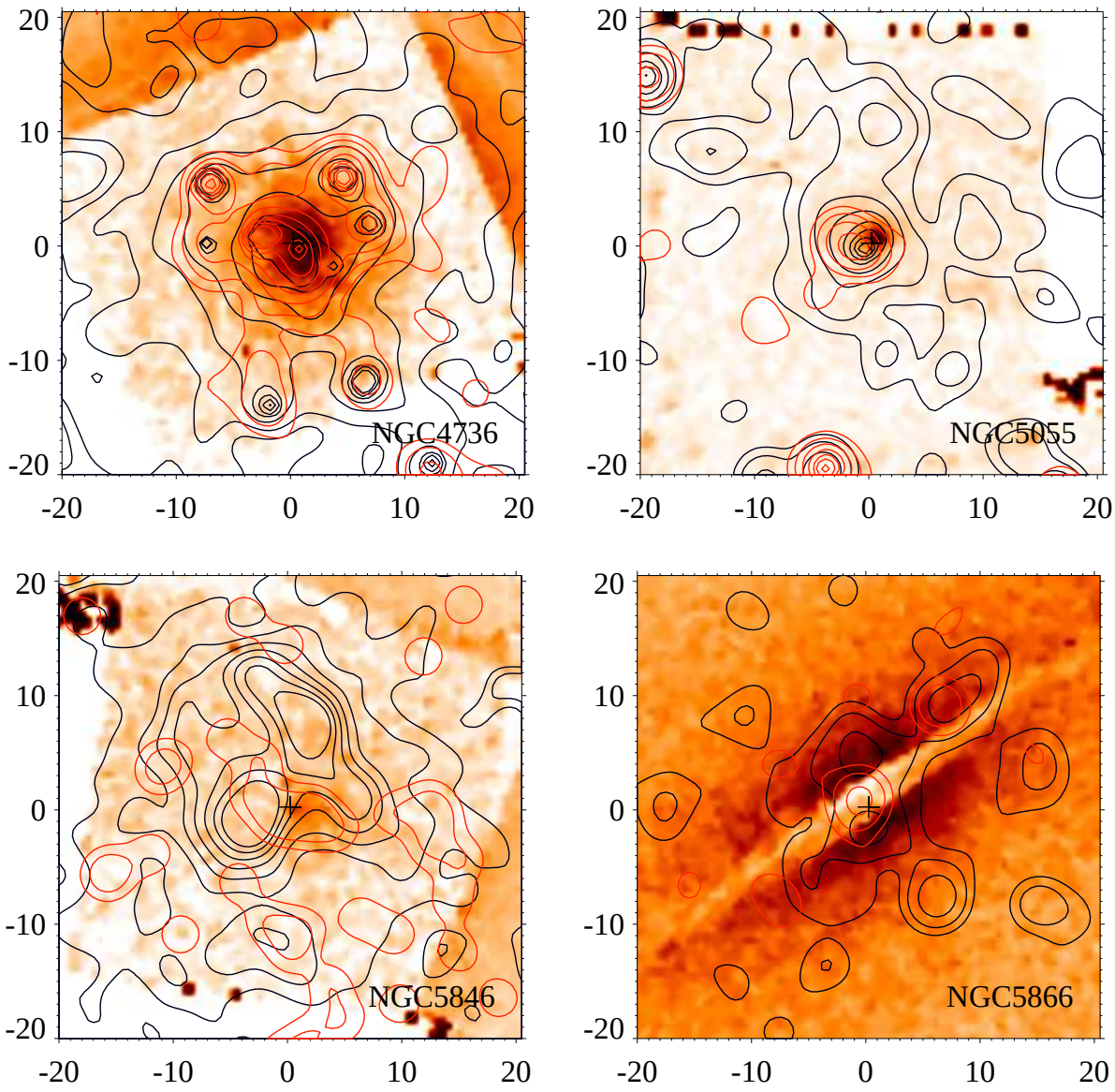

Fig. 6. Continued.